Interannual variability of the initiation of the phytoplankton growing period in two French coastal ecosystems

Main manuscript modifications are highlighted in red.

Coline Poppeschi[1], Guillaume Charria[1], Anne Daniel[2], Romaric Verney[3], Peggy Rimmelin-Maury[4], Michaël Retho[5], Eric Goberville[6], Emilie Grossteffan[4], Martin Plus[2]

[1]Ifremer, Univ. Brest, CNRS, IRD, Laboratory for Ocean Physics and Satellite remote sensing (LOPS), IUEM, 29280 Brest, France.
[2]Ifremer, DYNECO, Pelagic Ecology Laboratory (PELAGOS), 29280 Brest, France.
[3]Ifremer, DYNECO, Hydrosedimentary Dynamics Laboratory (DHYSED), 29280 Brest, France.
[4]OSU-European University Institute of the Sea (IUEM), UMS3113, 29280 Plouzané, France.
[5]Ifremer, Morbihan-Pays de Loire Environment Resources Laboratory (LERMPL), 56100 Lorient, France.
[6]Unité Biologie des Organismes et Ecosystèmes Aquatiques (BOREA), Muséum National d'Histoire Naturelle, CNRS, IRD, Sorbonne Université, Université de Caen Normandie, Université des Antilles, Paris, France

Correspondence to: Coline Poppeschi (coline.poppeschi@ifremer.fr)

Abstract. Decadal time series of chlorophyll-*a* concentrations sampled at high and low frequencies are explored to study climate-induced changes on the processes inducing interannual variations in the Initiation of the Phytoplankton Growing Period (IPGP) in early spring. In this study, we specifically detail the IPGP in two contrasting coastal temperate ecosystems under the influence of rivers highly rich in nutrients: the Bay of Brest and the Bay of Vilaine. A large interannual variability in the IPGP is observed in both ecosystems in connection with variations of environmental factors (available light depending from solar radiation, chlorophyll concentration and turbidity - sea temperature - turbulence driven by currents, wind direction and intensity and tidal mixing - nutrients from river flow). We show that the IPGP is delayed by around 30 days in 2019 in comparison with 2010. *In situ* observations and a one-dimensional vertical model coupling hydrodynamics, biogeochemistry, and sediment dynamics show that the IPGP generally depends on the interaction between several environmental factors. IPGP is mainly conditioned, at the local scale, by sea surface temperature and available light conditions, controlled by the turbidity of the system before first blooms. While both bays are hydrodynamically contrasted, the processes that modulate IPGP are similar. In both bays, IPGP can be delayed by cold spells and flood events at the end of winter if these extreme events last several days.

Keywords
Phytoplankton biomass, Long-term *in situ* observations, Coastal temperate ecosystems, Extreme events, Climate change.

1 Introduction

Although studied for 70 years (Sverdrup, 1953), the optimal conditions that trigger the Initiation of Phytoplankton Growing Period (IPGP) in ocean waters in early spring are not well understood (Sathyendranath *et al.,* 2015). Three main theories are proposed to date: the Critical Depth Hypothesis (Sverdrup, 1953), the Critical Turbulence Hypothesis (Huisman *et al.,* 1999) and the Disturbance-Recovery Hypothesis (Banse, 1994; Behrenfeld, 2010; Behrenfeld *et al.,* 2013). These hypotheses, determined with specific scales (e.g. mixed layer depth dynamics and annual evolution) and ecosystems, are still regularly debated owing to the use of more efficient models and new observation systems that allow the collection of large *in situ* datasets (Boss and Behrenfeld, 2010; Rumyantseva *et al.,* 2019; Caracciolo *et al*., 2021). Coastal waters remain highly dynamic and productive ecosystems at the interface between land and sea and are distinguished from the waters of the open sea (*e.g.* Gohin *et al.*, 2019; Liu *et al.*, 2019). Because coastal systems are directly influenced by anthropogenic inputs from rivers, no nutrient limitation is observed in late winter. A myriad of factors and mechanisms can then affect the IPGP in coastal areas (Townsend *et al.,* 1994; Cloern, 1996) but the incident light at the air/sea interface (Glé *et al.,* 2007) and the sea surface temperature (Trombetta *et al.,* 2019) are the main forcings. Low water turbidity also plays a major role and allows deeper light penetration (Iriarte and Purdie, 2004). This occurs by low vertical mixing conditions in shallow waters (Ianson *et al.*, 2001), i.e. limited advective exchanges, weak wind (Tian *et al.,* 2011),

neap tide (Ragueneau *et al.,* 1996) and in absence of flooding events (Peierls *et al.,* 2012). Depending on the morphology and hydrodynamics of coastal zones (estuaries, bays, lagoons), the importance of controlling factors can be variable (Cloern, 1996). The variability of IPGP plays a major role on several biological compartments in coastal ecosystems: change in the timing of IPGP can impact zooplankton and fish by inducing species replacements (Sommer *et al.,* 2012), or phytoplankton itself by changing species composition or the succession of species (Ianson *et al.,* 2001; Edwards and Richardson, 2004; Chivers *et al.,* 2020).

By amplifying or modifying environmental forcings, it is now well-documented that global climate change may influence the IPGP in coastal areas (Smetacek and Cloern, 2008; Barbosa *et al.,* 2010; Pearl *et al.,* 2014; IPCC, 2021). Heat waves, as opposed to cold spells, have become more frequent in recent years and can advance or delay the IPGP respectively (Gomez and Souissi, 2008). Wind storms, by inducing vertical mixing and sediment resuspension, can have a significant effect on water turbidity which in turn limits light penetration and therefore influences the IPGP. Floods, following heavier rainfall, may increase continental erosion, land-based transfers and ultimately nutrient inputs to coastal ecosystems. Because coastal ecosystems are strongly influenced by changes in land use, detecting long-term climate-induced signals is challenging (Krompkamp and Van Engeland, 2010).

Our study is based on two geographically close but hydrodynamically different nearshore ecosystems: (1) the Bay of Brest, a shallow semi-enclosed bay with well-mixed waters (Le Pape and Menesguen, 1997) and (2) the Bay of Vilaine, a shallow open bay with long water residence times (Chapelle *et al*., 1994). These two coastal ecosystems are strongly impacted by anthropogenic pressures, such as intensive agriculture (Ragueneau *et al.,* 2018; Ratmaya *et al.,* 2019). The river influence induces waters highly rich in nutrients. Most studies dealing with IPGP are mainly based on discrete water sampling (Iriarte *et al*., 2004; Tian *et al.*, 2011) or modeling (Townsend *et al.,* 1994; Philippart *et al.,* 2010). Only few studies investigate long-term high-frequency observations (Gomez and Souissi, 2008; Iriarte and Purdie, 2004) to assess interannual variability of the IPGP and to identify the triggering and controlling factors.

In this study, we aim to better understand interannual local changes in the IPGP in coastal temperate ecosystems in the current context of global climate change over the last 20 years. We first detect and analyze the temporal variability of the IPGP and we then quantify how environmental forcings influence its dynamics. To detect and analyze IPGP in coastal environments, we develop a method, combining high-frequency decadal *in situ* observations and modeling, based on a 1DV hydro-sedimentary and biogeochemical coupled numerical model. The potential impact of hydro-meteorological extreme events, such as cold waves, flood events and wind bursts, on the IPGP is then investigated.

2 Data and methods

2.1 Study areas

The study focuses on two northwestern French coastal temperate ecosystems, the Bay of Brest and the Bay of Vilaine, which are both impacted by excessive nutrient inputs from watersheds, but exposed to different hydrodynamic conditions.

The Bay of Brest is a semi-enclosed bay (180 km^2) with 50% of the surface shallower than 5 m depth. The Bay is connected with the Atlantic Ocean (Iroise sea) through a narrow and shallow strait. Tidal variation reaches 8 m during spring tides, which represents an oscillating volume of 40 % of the high tide volume. Freshwater inputs are essentially from the Aulne river (catchment area 1875 km^2, mean river flow 26 $m^3\ s^{-1}$), and also from two smaller rivers, the Elorn (catchment area 385 km^2, mean river flow 6 $m^3\ s^{-1}$) and the Mignonne (catchment area 111 km^2, mean river flow 1.5 $m^3\ s^{-1}$). Because of the macrotidal regime, the high nitrate concentrations do not generate important green tides (Le Pape et al., 1997) and the strong decreases in the Si:N and Si:P ratios did not exhibit dramatic phytoplankton community shifts from diatoms to non-siliceous species in spring (Del Amo *et al*., 1997) according to the high Si recycling (Ragueneau *et al*., 2002; Beucher *et al*, 2004).

The Bay of Vilaine is a mesotidal open bay (69 km^2) under the influence of the Vilaine (catchment area 10 500 km^2, mean river flow 70 $m^3\ s^{-1}$) and the Loire (catchment area 117 000 km^2, mean river flow 850 $m^3\ s^{-1}$) river discharges, with tidal ranges varying between 4 and 6 m (Merceron, 1985). The Loire river plume tends to spread northwestward with a dilution of 20- to 100-fold by the time it reaches the Bay of Vilaine (Ménesguen *et al*., 2018). The Vilaine river plume tends to spread throughout the bay before moving westward (Chapelle *et al*., 1994). The water residence time varies seasonally between 10 and 20 days (Chapelle *et al*., 1994). The water circulation is mainly driven by tides, winds and river flows (Lazure and Jegou, 1998). This bay is well known as one of the most sensitive European Atlantic coastal ecosystems to eutrophication (Ménesguen *et al*., 2019). The Bay of Vilaine has undergone eutrophication over recent decades mainly due to high nutrient inputs from the Vilaine and Loire rivers (Rossignol-Strick, 1985; Ratmaya *et al.*, 2019).

2.2 *In situ* observations

COAST-HF-Iroise (Rimmelin-Maury *et al*., 2020) and COAST-HF-Molit (Retho *et al*., 2020) are two high-frequency monitoring buoys of the French national observation network COAST-HF[1] (Répécaud *et al*., 2019; Farcy *et al*., 2019; Cocquempot *et al*., 2019; Poppeschi *et al*., 2021) located respectively in the Bay of Brest (4.582°W; 48.357°N) and in the Bay of Vilaine (2.660°W; 47.434°N) (Fig. 1). COAST-HF-Iroise has been operating in the strait between the Bay of Brest and the Iroise sea since 2000. COAST-HF-Molit buoy has been sampling the plume of the Vilaine river since 2008. Buoys are deployed during the whole year except for COAST-HF-Molit only available for part of the year prior to 2018 (from mid-February to early September, i.e. from day 50 to 250 for the period 2008-2017). Depending on the tide, the depth at the mooring sites ranges from 11 to 17 m for both COAST-HF buoys. Environmental parameters (temperature, salinity, turbidity, dissolved oxygen and Chl-*a* fluorescence) are measured at 2 m (COAST-HF-Iroise) and 1.3 m (COAST-HF-Molit) below the surface, every 20 and 60 minutes. The Chl-*a* fluorescence is measured by a Turner CYCLOPS-7 Sensor (precision $\pm$ 5%) and is considered as a proxy of phytoplankton biomass (unit FFU).

Sub-surface Chl-*a* concentrations are provided from two French marine monitoring networks, the SOMLIT coastal observation network[2] and the REPHY (French Observation and Monitoring program for Phytoplankton and Hydrology in coastal waters)[3]. They are collected bimonthly respectively at the SOMLIT-Brest (4.552°W; 48.358°N) and the REPHY-Loscolo (2.445°W; 47.496°N) stations which are close to the COAST-HF stations. Chlorophyll-*a* concentrations are measured with either spectrophotometric or fluorimetric methods (Aminot and Kérouel, 2004).

Daily river flows are measured at gauging stations (French hydrology "Banque Hydro" database[4]), located close to the main river mouths [Aulne-Gouezec (4.093°W; 48.205°N), Loire-Montjean (1.78°W; 47.106°N)]. The Vilaine river flow is controlled by a dam, and data were provided by the Vilaine Public Territorial Basin Organization[5] (Fig. 1).

The tide gauge stations (Shom[7]) at Brest (4.495°W; 48.382°N) and Crouesty (2.895°W; 47.542°N) record the sea level every minute.

Precipitation, air temperature, wind direction and intensity, and the solar flux data are retrieved every 6 minutes from two meteorological stations from the Météo-France observation network[6]: Guipavas (4.410°W; 48.440°N) and Vannes-Séné (2.425°W; 47.362°N) (Fig. 1). The solar flux can be used here as a proxy for subsurface PAR (Photosynthetically Available Radiation).

2.3 MARS3D-1DV modeling experiments

2.3.1 MARS3D-1DV model

A 1DV (one-dimensional vertical) model configuration is implemented to simulate changes in biogeochemical variables due to hydrodynamics and sediment dynamics in both bays.

The hydrodynamical model is based on the MARS3D (3D hydrodynamics Model for Applications at Regional Scale) code (Lazure and Dumas, 2008). This model is a primitive equation model with a free surface and uses the Boussinesq and hydrostatic pressure assumptions. Here, we use the 1DV configuration of the model, with 10 vertical sigma levels for 15 m depth. The time step is 30 s.

The sediment model (MUSTANG - Le Hir *et al.,* 2011; Grasso *et al.,* 2015; Mengual *et al.,* 2017) is designed to simulate the transport and changes in different sediment mixtures. In the sediment, 50 layers (refined near the surface) for a total thickness of 40 cm are implemented. Four sediment classes are considered: muds (diameter 10 μm), fine sand (diameter 100 μm), medium sand (diameter 200 μm) and coarse sand (diameter 400 μm). The sediment dynamics (transport in the water column, exchanges at the water/sediment interface, erosion/deposition

[1] www.coast-hf.fr, data available on www.coriolis-cotier.org

[2] https://somlit.fr

[3] https://doi.org/10.17882/47428

[4] www.hydro.eaufrance.fr/

[5] https://www.eptb-vilaine.fr/

[6] https://donneespubliques.meteofrance.fr/

[7] http://data.shom.fr

processes) are driven by an advection/dispersion equation for each sediment class (refer to Le Hir et al., 2011 for a detailed description of the sediment model).

The biogeochemical model BLOOM (BiogeochemicaL cOastal Ocean Model) is derived from the ECO-MARS model (Cugier *et al.,* 2005; Ménesguen *et al.,* 2019) adding major processes of early diagenesis. Nitrogen, phosphorus, and silica cycles are studied considering four nutrients, respectively nitrate, ammonium, soluble reactive phosphorus, silicic acid (sorption/desorption of phosphate on suspended sediment and precipitation/dissolution of phosphate with iron processes are also included). The model is also represented by three phytoplankton classes (microphytoplankton, dinoflagellates, pico-nano-phytoplankton), two zooplankton classes (micro- and meso-zooplankton), and exchanges at the water/sediment interface and inside the sediment compartment.

2.3.2 MARS3D-1DV model sensitivity experiments

These three models (hydrodynamical, sediment and biogeochemical) are coupled online during simulations and allow the nutrient and phytoplankton dynamics in both bays to be reproduced. The simulation for the Bay of Brest does not include nutrient inputs from the sediment because it is considered to be negligible around the COAST-HF-Iroise station.

Dissolved and particulate variables are defined in the water column and in the sediment. Initial values for both bays are uniform over the initial vertical profile (Table 1) and are based on a 3D realistic coupled simulation during the year 2015 the 15th of February extracted at the position of COAST-HF-Iroise for the Bay of Brest and at the position of COAST-HF-Molit station for the Bay of Vilaine (Plus *et a*l., 2021).

To evaluate the sensitivity of the biogeochemical dynamics to environmental conditions, sensitivity experiments are then performed using the coupled MARS3D/BLOOM/MUSTANG 1DV model configuration. All simulations are started at the end of winter (15th February) and run until the end of the year. The range of values used in the sensitivity experiments are derived from the minimum and maximum observed *in situ* data. Each parameter is tested with a constant value for the whole simulation.

Three parameters are individually explored in both bays:

- The air temperature in sensitivity experiments ranges from 4 to 14°C and is controlled by the intensity of solar radiations. Air temperature represents the main controlling parameter of Sea Surface Temperature in the 1DV model. This parameter drives the radiative fluxes in the model and then constrains the SST.
- Wind intensity effect on the IPGP is explored for values between 0 and 10 m s^{-1}. In the 1DV model, wind is a source of vertical mixing in the simulation.
- The Cloud Coverage (CC) sensitivity experiments ranged in value between 0 and 100% CC. This parameter is a driver of Photosynthetic Available Radiation (PAR) in the ocean. For the formulation of radiative fluxes in the 1DV MARS3D model, 100% cloud coverage allows an inflow of 38% of the total solar radiation in the water column. Each individual experiment is associated with a constant CC applied to the seasonal solar radiation.

As the sediment plays a role on the light penetration and acts as an active source of nutrients mainly in the Bay of Vilaine, the mud erosion rate (values between 2.10^{-5} and 2.10^{-7} kg m^{-2} s^{-1}) is explored only in that bay (sand erosion rate fixed to 0.0001 kg m^{-2} s^{-1}). For the sensitivity experiments, it drives a mass of sediment eroded and resuspended and a bottom input of nutrients in the water column.

A second set of experiments is conducted combining the effect of these environmental parameters in order to explore the cumulative or opposite effect on the IPGP. The upper and lower bounds of the range of environmental parameters are taken into account. Experiments are detailed in Table 5.

2.4 Data processing

2.4.1 Chl-*a* fluorescence data

To analyze high-frequency time series of *in situ* Chl-*a* fluorescence, the Quenching effect (Lehmuskero *et al*., 2018), a decrease in fluorescence in the presence of light (Fig. 2), is removed by analyzing only night-time data as reported in Carberry *et al*. (2019). Chl-*a* fluorescence data are studied on a daily basis, i.e. averaged from 10 pm to 5 am. Years with less than 75% of valid data (i.e. 2005, 2006, 2008, 2009 and 2018 in the Bay of Brest) are not considered.

2.4.2 Detection of the IPGP

We apply methods from the literature (Kromkamp *et al*., 2010; Philippart *et al*., 2010; Brody *et al*., 2013) to calculate annual IPGP values (not shown). Kromkamp *et al.* (2010) set an arbitrary beginning and end of the phytoplankton growing period at 20% and 80% of the cumulative Chl-a fluorescence measured from January 1st to December 31st. Similarly, Brody et al. (2013) consider a threshold of 5% above the yearly median chlorophyll. Philippart *et al.* (2010) considers the beginning of the growing period as the maximum daily difference in Chl-*a* fluorescence.

Because we obtain unrealistic IPGP dates from our dataset when using the methods proposed by Kromkamp *et al.* (2010 - i.e. too late IPGP); Brody *et al.* (2013 - i.e. too early IPGP) and Philippart *et al.* (2010 - i.e. multiple IPGP), we propose an alternative detection method based on discontinuities of the Chl-*a* fluorescence signal (Fig. 3): daily FFU slopes are calculated based on a linear regression over a +/-2 day window for each day, from 1st January to 31st December, and each year. The IPGP date is identified when the slope exceeds a threshold value, defined as the median of the daily slopes, for the first time in the year for at least 20 days. The end of the phytoplankton growing period is determined when the slope stabilizes below the threshold for at least 20 days for the last time in the year. The cumulative Chl-*a* fluorescence corresponds to the duration of the growing period.

2.4.3 Pattern of the phytoplankton growing period

The k-means method (Hartigan and Wong, 1979) is used to characterize the annual patterns of the phytoplankton growing period.

We exclude the year 2013 from the analysis of the Bay of Vilaine because of a large number of missing data. When the interval over which consecutive data are missing is no longer than one week, we perform a linear interpolation to replace the missing data. A 5-day running average is applied to the Chl-*a* fluorescence signal and the data are then normalized by the maximum value. We analyze Chl-*a* fluorescence every year for 150 days after the IPGP.

Time series from both bays are merged before application of the k-means and the number of clusters (or centroids) is set at 2 to distinguish the dominant patterns of the phytoplankton growth period at both sites. The use of a larger number of clusters is investigated and does not produce a pattern representing a large number of observed growing periods.

2.4.4 Detection of extreme events

The peak over threshold method (see Oliver *et al*., 2018 and Poppeschi *et al*., 2021 for further details) is used to detect hydro-meteorological extreme events such as cold waves, flood events and wind bursts. An event is considered as extreme if values are higher than a given statistical threshold for at least 3 consecutive days. In the present study, the 90-percentile threshold is selected to detect floods and wind bursts and the 10-percentile to detect cold waves. Seasonal anomalies are calculated over at least 20 years, by subtracting raw data from the winter average value (cold spells) or from the spring average value (wind bursts and floods).

3. Results

3.1 Characterization of the phytoplankton growing period

The high-frequency Chl-*a* fluorescence time series at both sites show an intense seasonal cycle with low values from November to February and high values from March to October (Fig. 4). Focusing on the period from 2010 to 2019 in the Bay of Brest, the minimum *Chl-a* fluorescence is observed during the years 2012 and 2013 and does not exceed 7 FFU. In contrast, years such as 2010, 2014, 2015 or 2019 show Chl-*a* fluorescence values above 15 FFU but can be up to 20 FFU. In the Bay of Vilaine, a similar seasonal pattern is observed with higher values reaching 50 FFU in 2013. Small (< 20 FFU) and high (> 35 FFU) Chl-*a* fluorescence amplitude are observed occasionally (in 2014 and 2017 and in 2013 and 2016, respectively). The Chl-*a* fluorescence is higher, almost double, in the Bay of Vilaine compared to the Bay of Brest with a mean cumulative Chl-*a* fluorescence around 580 FFU and 360 FFU, respectively (Table 2). The high phytoplankton biomass of the Bay of Vilaine is corroborated by the concentrations measured by low-frequency observation programs (SOMLIT and REPHY).

The phytoplankton growing period ranges from approximately March 10th to September 30th in both regions (Table 2). The average duration of the phytoplankton growing period is 179 days in the Bay of Vilaine and 200 days in the Bay of Brest (Table 2). The phytoplankton growing period is characterized by successive blooms, whose number and intensity are variable from year to year (Fig. 4).

The main patterns of the phytoplankton growing period are identified by the two clusters (Fig. 5). Cluster 0 includes the phytoplankton growing period with two successive marked blooms in early spring and in summer, the intensity of the second bloom being highly variable. Cluster 1 is characterized by a plateau during the two first months of the phytoplankton growing period. Most of the patterns of the Bay of Vilaine are in cluster 0 while those of the Bay of Brest are in cluster 1 (Table 3). The years that stand out in the Bay of Brest (2002, 2010, 2014) correspond to years with the highest cumulative *Chl-a* fluorescence ($\geq$ 450 FFU). The atypical years in the Bay of Vilaine (2011, 2017 and 2019) show the lowest cumulative *Chl-a* fluorescence ($\leq$ 450 FFU).

3.2 Variability of the Initiation of the Phytoplankton Growing Period (IPGP)

Calculations performed to determine the IPGP for high- and low-frequency data yield comparable results (Fig. 6). The mean differences between the IPGP calculated with the high and low-frequency data are 5 and 8 days for the Bay of Brest and the Bay of Vilaine, respectively. A difference of only 4 and 6 days between the model simulations (reference year = 2015) and the high-frequency *in situ* data is observed in the Bay of Brest and the Bay of Vilaine, respectively.

A decadal variability of the IPGP is recorded from mid-February to mid-April in both ecosystems (day 50 to day 102 in the Bay of Brest and day 53 to day 93 in the Bay of Vilaine; Fig. 6). In the Bay of Brest, early IPGPs (day < 53) are observed in 2010 and 2013 whereas late IPGP (day > 93) are observed in 2001, 2017 and 2019. In the Bay of Vilaine, the earliest IPGP is detected in 2012 (day 53) and the latest in 2019 (day 93).

The variability of IPGP in the Bay of Brest shows two linear trends (Fig. 6a), with a decrease of 52 days from 2001 to 2010 (observed in both high- and low-frequency datasets), followed by an increase (+48 days) from 2011 to 2019, a decline also observed in the Bay of Vilaine (Fig. 6b). Over the period 2011-2019, the IPGP is shifted towards a later date by +3.5 days per year in the Bay of Vilaine and +3.7 days per year in the Bay of Brest.

3.3 Analysis of environmental conditions driving the IPGP

3.3.1 Impact of environmental conditions on the IPGP

We next quantify the influence of environmental drivers on the date of IPGP (Fig. 7). These drivers represent the major limiting factors of the phytoplankton growth and comprise input of nutrients (river flow), PAR (incident light), Sea Surface Temperature - SST - (air temperature, incident light) and turbidity in the water column (river flow, wind intensity).

The median values of the environmental drivers observed at the date of each annual IPGP are very close in both bays (Table 4) : temperate SST (10 °C), weak wind (3 $m.s^{-1}$), a medium PAR (1360 W m^{-2}), a low turbidity (7 NTU) and a weak tidal amplitude (semi-amplitude of 1.6 m in the Bay of Brest and 0.9 m in the Bay of Vilaine). The IPGP occurs mainly during neap tides, at 68 % and 77 % in the Bay of Brest and in the Bay of Vilaine, respectively. The river flow is low during the IPGP with a runoff of 46 m^3 s^{-1} for the Aulne, 96 m^3 s^{-1} for the Vilaine and 1196 m^3 s^{-1} for the Loire.

To assess how environmental drivers may impact (i.e. advance or delay) the IPGP, we focus on the 15 days before the mean day of the IPGP (day 68) and of each annual IPGP. The considered 15 days length is related to the typical water residence time in both bays (Frere *et al.*, 2017; Poppeschi *et al.*, 2021 for the Bay of Brest - Chapelle *et al.*, 1994; Ratmaya *et al.*, 2019 for the Bay of Vilaine).

The earliest IPGP dates (IPGP < day 55) are associated with earlier occurrence of favorable environmental conditions than the other years. Earliest IPGP which occurred before day 55 are in 2010 and 2013 in the Bay of Brest and in 2012 in the Bay of Vilaine (Fig. S1f, 7c - S2a). Early IPGP between day 55 to 60, also associated with favorable environmental conditions, are found in 2002 and 2016 in the Bay of Brest (Fig. S1b, S1j).

In the same way, the latest IPGP dates (IPGP > day 90) are associated with unfavorable environmental conditions until the date of the IPGP. Latest IPGP occurring after day 90 are observed in 2001, 2003, 2017 and 2019 in the Bay of Brest and in 2019 in the Bay of Vilaine (Fig. S1a,c,k,l - S2g). For example, the delay detected in 2017 in both bays is due to strong wind and a lack of PAR until the day of IPGP (Fig. S1k - Fig. S2e). Late IPGP between day 70 to 90 are recorded in 2004, 2007 and 2012 in the Bay of Brest, and in 2014, 2017 and 2018 in the Bay of Vilaine (Fig. S1d,e,g, 7d - S2e,f).

The interannual variability of the date of the IPGP is therefore not controlled by a unique environmental driver. When the values of the environmental drivers responsible for the IPGP (Table 4) are compared to the mean values of the environmental drivers over a period of 30 days around the IPGP (Table S1), threshold values are observed in both bays: river flow is lower than usual (between 10 and 30 m^3 s^{-1}), temperature is close to the expected value (10°C), wind is weak (0.5 to 1.5 m s^{-1}), PAR is stronger (>300 W m^{-2}), and turbidity is low (about 1.5 NTU). IPGP starts around day 68 (±3 days) on average (Fig. 7a,b).

3.3.2 Modeling the importance of the environmental drivers

The relative contribution of each environmental driver on the IPGP is determined by MARS-1DV simulations starting on February 1st (Fig. 8). Environmental drivers tested in the model are controlling:

- the sea temperature - explored in the model by perturbing air temperature (as a controlling driver in the model of the Sea Surface Temperature evolution),
- the level of water turbulence - through wind intensity,
- the available light - controlled by Cloud Coverage (CC, as a sea surface PAR proxy) and turbidity (erosion rate as a proxy) limiting light penetration in the water column.

Model results show that early IPGP are associated with air temperature higher than 9 °C (resulting in a SST higher than 8 °C), low wind intensity, weak CC and low turbidity. Environmental drivers responsible for early or late IPGP are similar in both bays. Air temperature is the main driver with a potential deviation from the mean IPGP of 25 days in the Bay of Brest and 40 days in the Bay of Vilaine (Fig. 8). Wind, CC and turbidity have a lower impact on the IPGP (around 6 days in the Bay of Brest and 13 days in the Bay of Vilaine). In the Bay of Vilaine, the environmental drivers can simulate later IPGP than in the Bay of Brest.

In the Bay of Brest (Fig. 8a), only the air temperature variations have a real impact on the IGPG. If the air temperature is low (< 8°C), the IPGP is not triggered before day 74 (Table 5, Exp 1). If the air temperature is high (>13°C), the IPGP can start on day 49 (Table 5, Exp 2).

In the Bay of Vilaine, the air temperature and the erosion rate are the two main drivers impacting the IPGP (Fig. 8b). Similarly to the Bay of Brest, if the air temperature is low (< 6°C), the IPGP is late and appears only after day 80 (Table 5, Exp 1). If temperature is equal or above 13°C, the IPGP is early and appears on day 45 (Table 5, Exp 2). If the erosion rate is low (2.10^{-7} kg m^{-2} s^{-1}), then the IPGP takes place on day 76 (Table 5, Exp 7). If the erosion rate is high (2.10^{-5} kg m^{-2} s^{-1}), the IPGP occurs late after day 87 (Table 5, Exp 8).

The variations of wind and CC induce weaker shifts in the date of the IGPG, i.e. about one week at the most (Table 5, Exp 3,4,5,6). However, wind and CC can still explain variations of IPGP. For example, early IPGPs, in 2010 in the Bay of Brest and in 2012 in the Bay of Vilaine, due to low wind conditions (around 2 m s^{-1}, Fig. S2a - S1f) are observed in *in situ* measurements and also confirmed by the model (Fig. 8b).

The combined effect of the environmental factors can also be explored from the MARS-1DV model simulations (Fig. 9). The modeling conditions (hereafter called "Exp") are detailed in Table 5 and compared to the mean IPGP date (day 68).

The simulations confirm the observations, late IPGP correspond to the most extreme unfavorable combined environmental values (temperature of 4°C, wind intensity of 10 m s^{-1}, CC of 100% and erosion rate of 2.10^{-5} kg m^{-2} s^{-1} - Exp A). In the Bay of Brest and the Bay of Vilaine, IPGP occurs 9 days (i.e. twice as late as for any individual driver simulation) and 64 days later respectively. Late IPGP can also be linked to the combined effect of only two factors such as: "temperature and wind" and "temperature and CC" with a delay of 5 and around 22 days respectively (Exp B,C). In contrast, no delay is observed for the combination "wind and CC" (Exp D) in both bays.

Same as previously, early IPGP are found in the simulations as in the observations when conditions correspond to a high temperature (14°C), no wind intensity and CC, and a low erosion rate (2.10^{-7} kg m^{-2} s^{-1}) - Exp K. All the combined scenarios permit the occurrence of an earlier IPGP (by at least 5 additional days) compared to experiments that consider a single modified parameter.

This analysis enables environmental parameters to be classified with respect to their impact on the IPGP. In both bays, the temperature appears to be the key factor driving the IPGP. By combining the environmental drivers, the IPGP can occur even later or earlier than with a single forcing. In both bays, the combination of wind and CC has no impact on the IPGP, which occurs near the median day (Exp D and N). The extreme couplings of Exp A,E,F,G,J delay the date of IPGP later than detected in the observations for the Bay of Vilaine.All simulations show a higher impact on the date of IPGP in the Bay of Vilaine than in the Bay of Brest (Fig. 9, Table 5).

3.4 Impact of extreme hydro-meteorological events on the IPGP

3.4.1 Cold spells

The impact of cold spells on the IPGP is simulated with the MARS-1DV model based on two criteria: (i) the period of occurrence of the event, set in mid- or end February, (ii) the duration and intensity of the cold spell, which can be either short and weak (8 days, 7°C) or long and intense (20 days, 5°C) (Fig. 10).

In both bays, when the cold spell appears in mid-February, the IPGP is not impacted. However, it is delayed by about 15 days when occurring at the end of February. The duration of the cold spell, when longer than 15 days, also has an impact on the IPGP, with a delay of 13 and 12 days in the Bay of Brest and in the Bay of Vilaine, respectively.

Eight cold spells are detected in February in both bays between 2001 and 2019. In 2011, both sites are impacted simultaneously with cold spells. Long cold spells (30 days) are observed in 2009 and 2018, leading to an anomaly of more than -1.9°C.

The cold spell observed in 2018 in the Bay of Vilaine may explain the later IPGP. There is no change in the IPGP in 2011 and 2013, despite the cold spell, the period of occurrence being too early during winter 2011, and the duration too short in 2013 (only 10 days).

In the Bay of Brest, the cold spells in 2003 and 2004 may explain the delay of the IPGP (respectively days 93 and 85). The presence of long and intense cold spells in 2010 and 2011 do not shift the IPGP (days 50 and 67) because they occur too early (before day 20).

3.4.2 Wind bursts

Based on our model simulations, the wind bursts that occur during at least three continuous days have no impact on the IPGP in both bays, whatever the duration, the period and the intensity (+/- 1 day). In the Bay of Vilaine, only one wind event is detected in 2018 (3 days long and 6 $m.s^{-1}$). In the Bay of Brest, several events are detected, but no significant impact is observed on the IPGP.

3.4.3 Flood events

River floods can delay the IPGP by resuspending sediment in the water column and therefore limiting light penetration in the water column. Inputs of nutrients have no impact during the late winter period because nutrient concentrations are maximal, with no limitation on phytoplankton growth. Flood events are analyzed with observation data collected in the month prior to the IPGP date because the 1DV modeling approach does not allow the sensitivity to hydrological events to be simulated (*i.e.* it is necessary to simulate horizontal advection processes).

In the Bay of Brest, the impact of flood events depends on their duration and intensity: when the flood exceeds 15 days, a delay in the IPGP is detected. Shorter and more intense floods (> 300 $m^3\ s^{-1}$) do not impact the IPGP.

In the Bay of Vilaine, only two flood events are observed close to the IPGP date in 2014 and 2015. The 2015 flood event, which is 10 days longer and more intense (> 100 $m^3\ s^{-1}$) than the 2014 one, delays the IPGP date by 10 days.

4 Discussion

4.1 Comparison of the phytoplankton growing period in both bays

Despite their contrasting hydrodynamics (*e.g.* Petton *et al.*, 2020; Poppeschi *et al.*, 2021; Lazure and Jegou, 1998; Ratmaya *et al.*, 2019; Menesguen *et al.*, 2019), the median dates of the start and the end of the phytoplankton growing period are the same in the Bay of Brest and in the Bay of Vilaine whether they are calculated from high- and low- frequency datasets and from model simulations. The phytoplankton growing period occurs from March to September and lasts about 190 days in both bays. This concordance is related to a similar seasonality of the environmental drivers.

The observed cumulative fluorescence is almost double in the Bay of Vilaine compared with the Bay of Brest. This difference in the amount of chlorophyll produced in surface waters from both bays is also recorded by the low-frequency observation programs and by satellite observations (Menesguen *et al.*, 2019). It can be explained by the difference of the hydrodynamics and the influence of different watersheds. The Bay of Brest is a semi-enclosed bay with a macro-tidal regime influenced by two local rivers (Aulne and Elorn) whereas the Bay of Vilaine has a weaker tidal regime, is open on the continental shelf and is widely influenced by a large river (Loire river).

Two different patterns of the phytoplankton growing period are identified by the k-means classification in both bays. The flattened, weak and long bloom highlighted in the Bay of Brest can be explained by assuming that nutrients are not limiting the phytoplankton growth during spring. The maintenance of the diatom succession throughout spring since the 1980's (Quéguiner 1982; Del Amo *et al.*, 1997) can be explained by the combination of increasing N and P loads, intense Si recycling and a macrotidal regime (Ragueneau *et al.*, 2019). The phytoplankton growing period in the bay of Vilaine is characterized by several successive peaks including two main ones. Nutrients here drive the seasonal evolution of the phytoplankton growing period through periods of nutrient-limited conditions. These fluctuations are governed by phosphorus and nitrate loads from Vilaine and Loire rivers (Ratmaya *et al.*, 2019), but probably also by the stoichiometry of recycled elements in the water and at the water-sediment interface (Ratmaya *et al.*, 2022). However, at the beginning of the phytoplankton growing period (IPGP), the system is not nutrient limited in terms of nitrate, phosphorus and silicates.

4.2 Identification of the environmental conditions supporting the IPGP

The method that we developed to detect IPGP on both high-frequency and low-frequency *in situ* observations shows comparable results and detects similar initiation dates for some years, while a time lag between high- and low-frequency observations can be observed for other years. This difference is mainly explained by the difference in the sampling frequency. The late deployment of the buoy in the Bay of Vilaine (i.e. not deployed until mid-February before 2018) can also explain some differences between both sites. High-frequency data provide a more accurate detection of the day of the IPGP, while an uncertainty of about $\pm$ 7 days is observed with low-frequency observations. This comparison between high- and low-frequency based IPGP detection highlights the sensitivity of sampling strategy in the observation of phytoplankton growing periods (Bouman *et al.*, 2005; Serre-Fredj *et al.*, 2021) related to the response of the ecosystem within a few hours after an environmental change (Lefort and Gasol, 2014; Thyssen *et al.*, 2008).

The modeled IPGP, based on the year 2015, is coherent with high-frequency observations (around 5 days of difference between modeled and observed IPGP). Considering the idealized framework for modeling computations (1DV model instead of a realistic 3D model configuration), the agreement between observations and simulations validates the 1DV approach to explore IPGP dynamics. With the 1DV configuration, the vertical dynamics in the water column, coupled with biogeochemistry and sediment dynamics are well reproduced. Atmospheric forcings and interactions with the bottom layer are the main environmental drivers. The full range of impacts related to the horizontal advection (*e.g.* in considered regions, rivers advected plumes can change the hydrodynamics and the biogeochemical contents) are not evaluated, however. In the Bay of Brest and in the Bay of Vilaine, such advected sources exist (*e.g.* Poppeschi *et al.*, 2021; Lazure and Jegou, 1998) but inputs from rivers are not main drivers of the IPGP in nutrient-rich environments. Nutrient loads advected by rivers may impact the phytoplankton community later during the growing period rather than at IPGP (*e.g.* Ratmaya *et al.*, 2019).

We characterize similar environmental conditions in both bays as the IPGP is mainly driven and limited by similar local conditions. The ideal temperature (> 10°C) and PAR (1300 W m^{-2}) for the IPGP are in agreement with those from previous studies conducted in similar coastal ecosystems (*e.g.* Glé *et al.*, 2007; Townsend *et al.*, 1994; Trombetta *et al.*, 2019). Neap tidal conditions, weak wind (lower than 3 m s^{-1}) and weak river flow can also play a positive role to observe earlier IPGP according to the previous study of Ragueneau *et al.*, 1996.

As also shown in the German Bight (Tian *et al.*, 2011), wind intensity is a driver of turbidity in the water column which inhibits phytoplankton growth. The impact of wind direction on the IPGP is estimated to be negligible. Local changes in those features (temperature, incident radiation, tidal conditions, wind conditions and river flow) induce differences in detected IPGP. Indeed, in this coastal temperate ecosystem, we observe that the beginning of the growing period is limited by light (controlled by incident radiation, turbidity at this season), and water temperature. The IPGP also occurs during low vertical mixing conditions.

The comparison of the individual importance of each environmental driver shows that temperature and light penetration are the key environmental drivers in both bays. Similarly in the North Sea, Wiltshire *et al.* (2015) highlight the importance of the light availability in the timing and intensity of the spring bloom. Similarly, too high turbidity (due to sediment resuspension) can also limit the production and delay IPGP in the bay of Vilaine. Similar limitations are observed in the German Bight (Tian *et al.*, 2009) or along the UK South Coast (Iriarte and Purdie, 2004). The combined effect of surface incident radiation and turbidity can amplify the delay of the IPGP. However, with the existence of minimum mandatory conditions, an earlier IPGP can not be observed or modeled, except if thresholds are reached earlier (e.g. warmer temperature earlier during the year).

4.3 Interannual evolutions of the IPGP

The IPGP in these two bays shows a strong interannual variability with initiation dates varying from late winter to spring. A mean difference of 50 days between the earliest and latest IPGP dates is observed. Each year has a different date of IPGP related to different environmental conditions. However, the beginning of the phytoplankton growing period is always dominated in both bays by the same centric diatoms, genera *Chaetoceros* and *Skeletonema*, whose abundance varies from year to year depending on climatic conditions (REPHY, 2021).

The earliest IPGP are observed and related to favorable environmental conditions early in the year. For example, the IPGP can occur before day 50, associated with exceptionally weak wind and river flow in addition to a sufficient PAR and nearly-optimal temperature of around 10°C (e.g. 2010 in the Bay of Brest and 2012 in the Bay of Vilaine). But if the environmental conditions are not favorable (e.g. 2017 and 2019 in both bays), the IPGP is delayed. This can be due to a strong wind during several days (not a single wind burst) and a weak PAR and sometimes also because of turbidity events limiting the light penetration.

However, the reason to have early or late IPGP is not always the same. Late IPGP can be due to low temperature conditions rather than a strong wind or a lack of PAR as seen previously (e.g. 2003 in Bay of Brest). Also, the IPGP can be different from one bay to another in the same year, almost half of the years studied from 2012 to 2016. For example, the 2012 IPGP is early in the Bay of Vilaine (day 53) while it is late in the Bay of Brest (day 80), related to strong wind activity and low PAR. This difference between the two bays indicates a local, not regional, effect of the processes affecting the IPGP.

The analysis of the IPGP over the last two decades has highlighted its evolution through two trends, one per decade. The IPGP occurs earlier each year until 2010 when the trend is reversed. At a larger scale, this change in trends is not directly observed for the same years. For example, using hourly data, Hunter-Cervera *et al.* (2016) show earlier blooms of picophytoplankton on the New England Shelf during 2003-2012 due to warming spring periods, and later blooms in 2013-2015 for cooler spring temperatures. The similarity between these observations and those found here in our study on the other side of the Atlantic basin for a slightly later breaking year (2012 instead of 2010) suggests a large-scale impact of the warming waters in spring. On the eastern part of the Atlantic, we also know that 2010 was an atypical year, with an important accumulation of phytoplankton biomass as observed by Bedford *et al.* (2020) on the North-West European shelf. However, limited indicators do not allow conclusions to be drawn regarding the impact of large-scale forcings on observed shifts in phytoplankton blooms.

As the climate warms, earlier phytoplankton blooms are expected (Friedland *et al.*, 2018) but not later IPGP as observed in our study regions. However, the mechanisms that trigger blooms in coastal ecosystems - especially eutrophic ones - are not similar to the processes that influence blooms in the open ocean. For example, by investigating long-term (1975-2005) daily data, Wiltshire *et al.* (2008) observe later phytoplankton blooms in the German bight, but with no link to global warming. Henson *et al.* (2018) model a bloom shift of 5 days per decade from 2006 to 2025, with later blooms. A possible explanation may involve the lower spring sea surface temperatures, as observed in recent years (Hunter-Cervera *et al.* 2016), which could cause a delay of the IPGP. We do not detect significant trends in environmental conditions over the last 20 years at either site, and therefore do not establish direct links with the trends observed in the IPGP timing. In the southern California Bight, similar changes in IPGP are observed from 1983 to 2000, but no link with environmental drivers has been identified (Kim *et al.*, 2009).

4.4 Extreme events

We show that a cold spell is likely to delay the IPGP if it occurs at the end of winter (after 20th February) or/and if the cold spell lasts long enough (> 15 days). This is in accordance with the study of Gomez and Souissi (2008) in the English Channel where cold spells can affect the date of IPGP by increasing the water column mixing. In both bays, the drop in temperature related to the cold spell prevents the IPGP. Cold spells may also drive local patterns by influencing the phytoplankton communities (Gomez and Souissi, 2008; Schlegel *et al*., 2021).

Flood events have an influence on the phytoplankton biomass when they occur in spring due to the supply of nutrients. When they occur in late winter, nutrients are already at their maximum. The impact of floods on IPGP is consequent only if they are at least 15 days long. This scheme is also observed by Saeck *et al*. (2013) along a river-estuary-bay continuum and explained by a shortened water residence time and a limited light due to flood-induced turbidity in the coastal zone.

No relationship is observed between wind events and IPGP in both bays because they are weakly stratified contrary to open seas (*i.e*. Black Sea, Mikaelyan *et al*., 2017). In coastal stratified regions (e.g. under the influence of river plumes), strong wind and tidal mixing can enhance the mixing and break down stratification thus distributing phytoplankton (Joordens et al., 2021). During the IPGP, except during floods, both regions are weakly stratified and are then less sensitive to combined wind/tidal short events.

5 Conclusions

This study provides a new understanding of the IPGP dynamics in coastal temperate areas by using both high and low-frequency *in situ* data, in combination with simulations from a 1DV model. Strong similarities are found in both bays. An important interannual variability of the IPGP is observed, with a trend towards a later IPGP over the last decade (2010-2020). We quantify the importance of environmental conditions on the IPGP. When we compare observed IPGP with favorable environmental conditions and following sensitivity experiments with the 1DV model, water temperature and turbidity (limiting light penetration in the water column) appear as the main drivers explaining interannual IPGP variability. The IPGP is a complex mechanism, usually triggered by more than one environmental parameter. The analysis of the influence of extreme events reveals that cold spells and floods have a strong impact by delaying the IPGP when episodes are long enough and occur after winter. No effect of wind bursts is detected.

While this study shows comparable IPGP dynamics when based on 1DV model simulations or *in situ* observations, we will next investigate the effect of a fully realistic hydrodynamics (including horizontal and vertical advections; mixing processes; remote sources of nutrients from rivers) on phytoplankton dynamics using a 3D model. We will focus on exploring the variability of phytoplankton communities during IPGP to assess whether community change is occurring, as observed in other studies and for other ecosystems (Ianson et al., 2001; Edwards and Richardson, 2004; Chivers et al., 2020). When interannual evolutions in the phytoplankton growth are explored, the detection and the understanding of harmful algal bloom dynamics can also be addressed based on similar approaches. Further studies will be dedicated to the simulation of the coastal ecosystem in the future based on numerical simulation based on climate scenarios. The investigation of other contrasting coastal environments will allow us to better understand and anticipate the expected impact of global change on coastal phytoplankton dynamics.

Author contributions

CP, GC, AD, RV, PR-M and EGo conceptualized the study. PR-M, EGr and MR collected data. MP and GC developed the model configuration. CP, GC, AD and RV drafted the first versions of the paper. CP carried out all the analyses and wrote the final version of the paper. All authors contributed to the discussions and revisions of the study.

Acknowledgements

We would like to acknowledge COAST-HF (http://www.coast-hf.fr), SOMLIT (http://somlit.epoc.u-bordeaux1.fr) and REPHY (https://doi.org/10.17882/47248) national observing networks, for providing data flux readily available. COAST-HF and SOMLIT are components of the National Research Infrastructure ILICO. We would like to thank the Shom for tidal data and also Météo-France for wind and solar flux products. We also thank Dr Claire Labry for fruitful discussions and Dr Sally Close for her proofreading.

Financial support

This study is part of the State-Region Plan Contract ROEC supported in part by the European Regional Development Funds and the COXTCLIM project funded by the Loire-Brittany Water Agency, the Brittany region and Ifremer.

References

Aminot, A., and Kerouel, R.: Hydrologie des écosystèmes marins. Paramètres et analyses, Editions de l'Ifremer, 336 p., ISBN 2-84433-133-5, 2004.

Banse, K.: Grazing and zooplankton production as key controls of phytoplankton production in the open ocean, *Oceanography*, *7*(1), 13-20, https://www.jstor.org/stable/43925524, 1994.

Barbosa, A., Domingues, R., and Galvão., H.: Environmental forcing of phytoplankton in a Mediterranean estuary (Guadiana estuary, south-western Iberia): A decadal study of anthropogenic and climatic influences, Estuaries and Coasts, doi:10.1007/ s12237-009-9200-x, 2010.

Bedford, J., Ostle, C., Johns, D. G., Atkinson, A., Best, M., Bresnan, E., ... and McQuatters-Gollop, A.: Lifeform indicators reveal large-scale shifts in plankton across the North-West European shelf, *Global Change Biology*, *26*(6), 3482-3497, doi:10.1111/gcb.15066, 2020.

Behrenfeld, M. J.: Abandoning Sverdrup's critical depth hypothesis on phytoplankton blooms, *Ecology*, *91*(4), 977-989, doi:10.1890/09-1207, 2010.

Behrenfeld, M. J., Doney, S. C., Lima, I., Boss, E. S., and Siegel, D. A.: Annual cycles of ecological disturbance and recovery underlying the subarctic Atlantic spring plankton bloom, *Global biogeochemical cycles*, *27*(2), 526-540, doi:10.1002/gbc.20050, 2013.

Beucher, C., Treguer, P., Corvaisier, R., Hapette, A. M., and Elskens, M.: Production and dissolution of biosilica, and changing microphytoplankton dominance in the Bay of Brest (France), *Marine Ecology Progress Series*, *267*, 57-69, doi:10.3354/meps267057, 2004.

Boss, E., and Behrenfeld, M.: In situ evaluation of the initiation of the North Atlantic phytoplankton bloom, *Geophysical Research Letters*, *37*(18), doi:10.1029/2010GL044174, 2010.

Bouman, H., Platt, T., Sathyendranath, S., and Stuart, V.: Dependence of light-saturated photosynthesis on temperature and community structure, *Deep Sea Research Part I: Oceanographic Research Papers*, *52*(7), 1284-1299, doi:10.1016/j.dsr.2005.01.008, 2005.

Brody, S. R., Lozier, M. S., and Dunne, J. P.: A comparison of methods to determine phytoplankton bloom initiation, *Journal of Geophysical Research, Oceans*, *118*(5), 2345-2357, doi:10.1002/jgrc.20167, 2013.

Caracciolo, M., Beaugrand, G., Hélaouët, P., Gevaert, F., Edwards, M., Lizon, F., ... and Goberville, E.: Annual phytoplankton succession results from niche-environment interaction, *Journal of Plankton Research*, *43*(1), 85-102, doi:10.1093/plankt/fbaa060, 2021.

Chapelle, A., Lazure, P., and Ménesguen, A.: Modelling eutrophication events in a coastal ecosystem. Sensitivity analysis, *Estuarine, Coastal and Shelf Science*, *39*(6), 529-548, doi:10.1016/S0272-7714(06)80008-9, 1994.

Chivers, W. J., Edwards, M., and Hays, G. C.: Phenological shuffling of major marine phytoplankton groups over the last six decades, *Diversity and Distributions*, *26*(5), 536-548, doi:10.1111/ddi.13028, 2020.

Cloern, J. E.: Phytoplankton bloom dynamics in coastal ecosystems: a review with some general lessons from sustained investigation of San Francisco Bay, California, *Reviews of Geophysics*, *34*(2), 127-168, doi:10.1029/96RG00986, 1996.

638 Cocquempot, L., Delacourt, C., Paillet, J., Riou, P., Aucan, J., Castelle, B., Charria, G., Claudet, J., Conan, P.,
639 Coppola, L., Hocdé, R., Planes, S., Raimbault, P., Savoye, N., Testut, L., and Vuillemin, R.: Coastal Ocean and
640 Nearshore Observation: A French Case Study, Frontiers in Marine Science, 6(324), 1-17,
641 doi:10.3389/fmars.2019.00324, 2019.
642
643 Cook, P. L., Holland, D. P., and Longmore, A. R.: Effect of a flood event on the dynamics of phytoplankton and
644 biogeochemistry in a large temperate Australian lagoon, *Limnology and Oceanography*, *55*(3), 1123-1133,
645 doi:10.4319/lo.2010.55.3.1123, 2010.
646
647 Cugier, P., Billen, G., Guillaud, J. F., Garnier, J., and Ménesguen, A.: Modelling the eutrophication of the Seine
648 Bight (France) under historical, present and future riverine nutrient loading, *Journal of Hydrology*, *304*(1-4), 381-
649 396, doi:10.1016/j.jhydrol.2004.07.049, 2005.
650
651 Del Amo, Y., Le Pape, O., Tréguer, P., Quéguiner, B., Ménesguen, A., and Aminot, A.: Impacts of high-nitrate
652 freshwater inputs on macrotidal ecosystems. I. Seasonal evolution of nutrient limitation for the diatom-dominated
653 phytoplankton of the Bay of Brest (France), *Marine Ecology Progress Series*, *161*, 213-224, doi:10.5194/bg-16-
654 1361-2019, 1997.
655
656 Edwards, M., and Richardson, A. J.: Impact of climate change on marine pelagic phenology and trophic
657 mismatch, *Nature*, *430*(7002), 881-884, doi:10.1038/nature02808, 2004.
658
659 Farcy, P., Durand, D., Charria, G., Painting, S.J., Tamminem, T., Collingridge, K., Grémare, A.J., Delauney, L.,
660 and Puillat, I.: Toward a European coastal observing network to provide better answers to science and to societal
661 challenges; the JERICO research infrastructure, Frontiers in Marine Science, 6, 1–13,
662 doi:10.3389/fmars.2019.00529, 2019.
663
664 Frère, L., Paul-Pont, I., Rinnert, E., Petton, S., Jaffré, J., Bihannic, I., Soudant, P., Lambert, C. and Huvet, A.:
665 Influence of environmental and anthropogenic factors on the composition, concentration and spatial distribution
666 of microplastics : a case study of the Bay of Brest (Brittany, France), Environ. Pollut, 225, 211–222,
667 doi:10.1016/j.envpol.2017.03.023, 2017.
668
669 Friedland, K. D., Mouw, C. B., Asch, R. G., Ferreira, A. S. A., Henson, S., Hyde, K. J., ... and Brady, D. C.:
670 Phenology and time series trends of the dominant seasonal phytoplankton bloom across global scales, *Global*
671 *Ecology and Biogeography*, *27*(5), 551-569, doi:10.1111/geb.12717, 2018.
672
673 Glé, C., Del Amo, Y., Bec, B., Sautour, B., Froidefond, J. M., Gohin, F., Maurer, D., Plus, M., Laborde, P., and
674 Chardy, P.: Typology of environmental conditions at the onset of winter phytoplankton blooms in a shallow
675 macrotidal coastal ecosystem, Arcachon Bay (France), *Journal of plankton research*, *29*(11), 999-1014,
676 doi:10.1093/plankt/fbm074, 2007.
677
678 Gohin, F., Van der Zande, D., Tilstone, G., Eleveld, M. A., Lefebvre, A., Andrieux-Loyer, F., Blauw, A. N.,
679 Bryère, P., Devreker, D., Garnesson, P., Hernández Fariñas, T., Lamaury, Y., Lampert, L., Lavigne, H., Menet-
680 Nedelec, F., Pardo, S., and Saulquin, B.: Twenty years of satellite and in situ observations of surface chlorophyll-
681 a from the northern Bay of Biscay to the eastern English Channel. Is the water quality improving ? *Remote Sensing*
682 *of Environment*, *233*(September), 111343, doi:10.1016/j.rse.2019.111343, 2019.
683
684 Gomez, F., and Souissi, S.: The impact of the 2003 heat wave and the 2005 cold wave on the phytoplankton in the
685 north-eastern English Channel, Comptes Rendues Biologies, 331(9), 678-685, doi:10.1016/j.crvi.2008.06.005,
686 2008.

687 Grasso F., Le Hir P., and Bassoullet P.: Numerical modelling of mixed-sediment consolidation, *Ocean Dynamics*,
688 65(4), 607– 616, doi:10.1007/s10236-015-0818-x, 2015.

689 Hartigan, J., and Wong, M.: Algorithm AS 136: A K-Means Clustering Algorithm. Journal of the Royal Statistical
690 Society, Series C (Applied Statistics), 28:1, 100-108, doi:2346830, 1979.
691
692 Henson, S. A., Cole, H. S., Hopkins, J., Martin, A. P., and Yool, A.: Detection of climate change-driven trends in
693 phytoplankton phenology, *Global Change Biology*, *24*(1), e101-e111, doi:10.1111/gcb.13886, 2018.

Huisman, J. E. F., van Oostveen, P., and Weissing, F. J.: Critical depth and critical turbulence: two different mechanisms for the development of phytoplankton blooms, *Limnology and oceanography*, *44*(7), 1781-1787, doi.org/10.4319/lo.1999.44.7.1781, 1999.

Hunter-Cevera, K. R., Neubert, M. G., Olson, R. J., Solow, A. R., Shalapyonok, A., and Sosik, H. M.: Physiological and ecological drivers of early spring blooms of a coastal phytoplankter, *Science*, *354*(6310), 326-329, doi:10.1126/science.aaf8536, 2016.

Husson, B., Hernández-Fariñas, T., Le Gendre, R., Schapira, M., and Chapelle, A.: Two decades of Pseudo-nitzschia spp. blooms and king scallop (Pecten maximus) contamination by domoic acid along the French Atlantic and English Channel coasts: Seasonal dynamics, spatial heterogeneity and interannual variability, *Harmful Algae*, *51*, 26-39, doi:10.1016/j.hal.2015.10.017, 2016.

Ianson, D., Pond, S., and Parsons, T.: The spring phytoplankton bloom in the coastal temperate ocean: growth criteria and seeding from shallow embayments, *Journal of oceanography*, *57*(6), 723-734, doi.org/10.1023/A:1021288510407, 2001.

IPCC: Summary for Policymakers. In: *Climate Change 2021: The Physical Science Basis. Contribution of Working Group I to the Sixth Assessment Report of the Intergovernmental Panel on Climate Change* [Masson-Delmotte, V., P. Zhai, A. Pirani, S. L. Connors, C. Péan, S. Berger, N. Caud, Y. Chen, L. Goldfarb, M. I. Gomis, M. Huang, K. Leitzell, E. Lonnoy, J.B.R. Matthews, T. K. Maycock, T. Waterfield, O. Yelekçi, R. Yu and B. Zhou (eds.)], Cambridge University Press, In Press, 2021.

Iriarte, A., and Purdie, D. A.: Factors controlling the timing of major spring bloom events in an UK south coast estuary, *Estuarine, Coastal and Shelf Science*, *61*(4), 679-690, doi:10.1016/j.ecss.2004.08.002, 2004.

Joordens, J. C. A., Souza, A. J., & Visser, A.: The influence of tidal straining and wind on suspended matter and phytoplankton distribution in the Rhine outflow region. *Continental Shelf Research*, *21*(3), 301-325, doi:10.1016/S0278-4343(00)00095-9, 2001.

Kromkamp, J. C., and Van Engeland, T.: Changes in phytoplankton biomass in the western Scheldt estuary during the period 1978-2006, *Estuaries and Coasts*, *33*(2), 270–285, doi:10.1007/s12237-009-9215-3, 2010.

Kim, H. J., Miller, A. J., McGowan, J., and Carter, M. L.: Coastal phytoplankton blooms in the Southern California Bight, *Progress in Oceanography*, *82*(2), 137-147, doi:10.1016/j.pocean.2009.05.002, 2009.

Lazure, P., and Dumas, F.: An external–internal mode coupling for a 3D hydrodynamical model for applications at regional scale (MARS), *Advances in water resources*, *31*(2), 233-250, doi:10.1016/j.advwatres.2007.06.010, 2008.

Lazure, P., and Jégou, A. M.: 3D modelling of seasonal evolution of Loire and Gironde plumes on Biscay Bay continental shelf, *Oceanologica acta*, *21*(2), 165-177, doi:10.1016/S0399-1784(98)80006-6, 1998.

Lefort, T., and Gasol, J. M.: Short-time scale coupling of picoplankton community structure and single-cell heterotrophic activity in winter in coastal NW Mediterranean Sea waters, *Journal of plankton research*, *36*(1), 243-258, doi:10.1093/plankt/fbt073, 2014.

Le Hir P., Cayocca F., and Waeles B.: Dynamics of sand and mud mixtures: A multiprocess-based modelling strategy, *Continental Shelf Research*, 31(10), S135– S149, doi:10.1016/j.csr.2010.12.009, 2011.

Lehmuskero, A., Skogen Chauton, M., and Boström, T.: Light and photosynthetic microalgae: A review of cellular- and molecular-scale optical processes, *Progress in Oceanography*, *168*(September), 43–56, doi:10.1016/j.pocean.2018.09.002, 2018.

Le Pape, O., and Menesguen, A.: Hydrodynamic prevention of eutrophication in the Bay of Brest (France), a modelling approach, *Journal of Marine Systems*, *12*(1-4), 171-186, doi:10.1016/S0924-7963(96)00096-6, 1997.

748 Liu, X., Dunne, J. P., Stock, C. A., Harrison, M. J., Adcroft, A., and Resplandy, L.: Simulating water residence
749 time in the coastal ocean: A global perspective, *Geophysical Research Letters*, *46*(23), 13910-13919, doi:
750 10.1029/2019GL085097, 2019.
751
752 Ménesguen, A., Dussauze, M., and Dumas, F.: Designing optimal scenarios of nutrient loading reduction in a
753 WFD/MSFD perspective by using passive tracers in a biogeochemical-3D model of the English Channel/Bay of
754 Biscay area, *Ocean & Coastal Management*, *163*, 37-53, doi:10.1016/j.ocecoaman.2018.06.005, 2018.
755
756 Ménesguen, A., Dussauze, M., Dumas, F., Thouvenin, B., Garnier, V., Lecornu, F., and Répécaud, M.: Ecological
757 model of the Bay of Biscay and English Channel shelf for environmental status assessment part 1: Nutrients,
758 phytoplankton and oxygen, *Ocean Modelling*, *133*, 56-78, doi.org/10.1016/j.ocemod.2018.11.002, 2019.

759 Mengual B., Le Hir P., Cayocca F., and Garlan T.: Modelling fine sediment dynamics: Towards a common erosion
760 law for fine sand, mud and mixtures, *Water*, 9, 564, doi:10.3390/w9080564, 2017.

761 Mikaelyan, A., Chasovnikov, V., Kubryakov, A., and Stanichny, S.: Phenology and drivers of the winter-spring
762 phytoplankton bloom in the open Black Sea: The application of Sverdrup's hypothesis and its refinements,
763 Progress in Oceanography, 151, 163-176, doi:10.1016/j.pocean.2016.12.006, 2017.

764 Monchevaa, S., Gotsis-Skretasb, O., Pagoub, K., and Krasteva, A.: Phytoplankton Blooms in Black Sea and
765 Mediterranean Coastal Ecosystems Subjected to Anthropogenic Eutrophication: Similarities and
766 Differences, *Estuarine, Coastal and Shelf Science*, *53*, 281-295, doi:10.1006/ecss.2001.0767, 2001.
767
768 Oliver, E., Donat, M., Burrows, M., Moore, P., Smale, D., Alexanda, L., Benthuysen, J., Feng, M., Sen Gupta, A.,
769 Hobday, A., Holbrook, N., Perkins-Kirkpatrick, S., Scannell, H., Straub, S. and Wernberg, T.: Longer and more
770 frequent marine heatwaves over the past century, Nature communications, 9 :1324, doi:10.1038/s41467-018-
771 03732-9, 2018.
772
773 Paerl, H. W., Hall, N. S., Peierls, B. L., and Rossignol, K. L.: Evolving paradigms and challenges in estuarine and
774 coastal eutrophication dynamics in a culturally and climatically stressed world, *Estuaries and coasts*, *37*(2), 243-
775 258, doi.org/10.1007/s12237-014-9773-x, 2014.
776
777 Peierls, B. L., Hall, N. S., and Paerl, H. W.: Non-monotonic responses of phytoplankton biomass accumulation to
778 hydrologic variability: a comparison of two coastal plain North Carolina estuaries, *Estuaries and coasts*, *35*(6),
779 1376-1392, doi.org/10.1007/s12237-012-9547-2, 2012.
780
781 Petton, S., Pouvreau, S., and Dumas, F. Intensive use of Lagrangian trajectories to quantify coastal area dispersion,
782 Ocean Dynamics, 70(4), 541-559, doi.org/10.1007/s10236-019-01343-6, 2020.
783
784 Philippart, C. J. M., van Iperen, J. M., Cadée, G. C., and Zuur, A. F.: Long-term field observations on seasonality
785 in chlorophyll-a concentrations in a shallow coastal marine ecosystem, the Wadden Sea, Estuaries and Coasts,
786 33(2), 286–294, doi:10.1007/s12237-009-9236-y, 2010.
787
788 Plus, M., Thouvenin, B., Andrieux, F., Dufois, F., Ratmaya, W., Souchu, P. Diagnostic étendu de l'eutrophisation
789 (DIETE). Modélisation biogéochimique de la zone Vilaine-Loire avec prise en compte des processus
790 sédimentaires. Description du modèle Bloom (BiogeochemicaL cOastal Ocean Model). RST/LER/MPL/21.15.
791 https://archimer.ifremer.fr/doc/00754/86567/, 2021.
792
793 Poppeschi, C., Charria, G., Goberville, E., Rimmelin-Maury, P., Barrier, N., Petton, S., Unterberger, M.,
794 Grossteffan, E., Repeccaud, M., Quéméner, L., Le Roux, J.-F., and Tréguer, P.: Unraveling salinity extreme events
795 in coastal environments : a winter focus on the bay of Brest, Frontiers in Marine Science, 8,
796 705403, doi:10.3389/fmars.2021.705403, 2021.
797
798 Quéguiner, B., and Tréguer, P.: Studies on the Phytoplankton in the Bay of Brest (Western Europe), Seasonal
799 Variations in Composition, Biomass and Production in Relation to Hydrological and Chemical Features (1981—
800 1982), Botanica Marina, 27, 449-459, 1984.
801
802 Ragueneau, O., Quéguiner, B. and Tréguer, P.: Contrast in biological responses to tidally-induced vertical mixing
803 for two macrotidal ecosystems of western Europe, Estuarine, Coastal and Shelf Science, 42, 645-665,
804 doi:10.1006/ecss.1996.0042, 1996.

Ragueneau, O., Chauvaud, L., Leynaert, A., Thouzeau, G., Paulet, Y. M., Bonnet, S., Lorrain, A., Grall, J., Corvaisier, R., Le Hir, M., Jean, F., and Clavier, J.: Direct evidence of a biologically active coastal silicate pump: ecological implications, *Limnology and Oceanography*, *47*(6), 1849-1854, doi.org/10.4319/lo.2002.47.6.1849, 2002.

Ragueneau, O., Raimonet, M., Mazé, C., Coston-Guarini, J., Chauvaud, L., Danto, A., Grall, J., Jean, F., Paulet Y.-M., and Thouzeau, G.: The impossible sustainability of the Bay of Brest ? Fifty years of ecosystem changes, interdisciplinary knowledge construction and key questions at the science-policy-community interface, *Frontiers in Marine Science*, *5*, 124, doi.org/10.3389/fmars.2018.00124, 2018.

Ratmaya, W., Soudant, D., Dalmon-Monviola, J., Plus, M., Cochennec-Laureau, N., Goubert, E., Andrieux-Loyer, F., Barillé, L. and Souchu, P.: Reduced phosphorus loads from the Loire and Vilaine rivers were accompanied by increasing eutrophication in the Vilaine Bay (south Brittany, France), Biogeosciences, 16:1361-1380, doi:10.5194/bg-16-1361-2019, 2019.

Ratmaya, W., Laverman, AM., Rabouille, C., Akbarzadeh, Z., Andrieux-Loyer, F., Barillé, L., Barillé, A-L., Le Merrer, Y., and Souchu, P.: Temporal and spatial variations in benthic nitrogen cycling in a temperate macro-tidal coastal ecosystem : Observation and modeling, *Continental Shelf Research*, doi:10.1016/j.csr.2022.104649, 2022.

Répécaud, M., Quemener, L., Charria, G., Pairaud, I., Rimmelin, P., Claquin, P., Jacqueline, F., Lefebvre, A., Facq, J.V., Retho, M., and Verney, R.: National observation infrastructure: an example of a fixed-platforms network along the French Coast: COAST HF, OCEANS IEE, pp. 1-6, doi:10.1109/OCEANSE.2019.8867451, 2019.

REPHY: French Observation and Monitoring program for Phytoplankton and Hydrology in coastal waters, REPHY dataset - French Observation and Monitoring program for Phytoplankton and Hydrology in coastal waters. Metropolitan data, SEANOE, doi:10.17882/47248, 2021.

Retho, M., Quemener, L., Le Gall, C., Repecaud, M., Souchu, P., Gabellec, R. and Manach, S.: MOLIT Vilaine data and metadata from Coriolis Data Centre, SEANOE, doi:10.17882/46529, 2020.

Rimmelin-Maury, P., Charria, G., Repecaud, M., Quemener, L., Beaumont, L. Guillot, A., Gautier, L., Prigent, S., Le Becque, T., Bihannic, I., Bonnat, A., Le Roux, J-F., Grossteffan, E., Devesa, J., and Bozec, Y.: Iroise buoys data from Coriolis data center as core parameter support for Brest Bay and Iroise sea studies, SEANOE, 2020.

Rossignol-Strick, M.: A marine anoxic event on the Brittany coast, July 1982, *Journal of Coastal Research*, 11-20, https://www.jstor.org/stable/4297005, 1985.

Rumyantseva, A., Henson, S., Martin, A., Thompson, A. F., Damerell, G. M., Kaiser, J., and Heywood, K. J.: Phytoplankton spring bloom initiation: The impact of atmospheric forcing and light in the temperate North Atlantic, Ocean. *Progress in oceanography*, *178*, 102202, doi:10.1016/j.pocean.2019.102202, 2019.

Saeck, E. A., Hadwen, W. L., Rissik, D., O'Brien, K. R., and Burford, M. A.: Flow events drive patterns of phytoplankton distribution along a river–estuary–bay continuum, *Marine and Freshwater Research*, *64*(7), 655-670, doi:10.1071/MF12227, 2013.

Sathyendranath, S., Ji, R., and Browman, H. I.: Revisiting Sverdrup's critical depth hypothesis, *ICES Journal of Marine Science*, *72*(6), 1892-1896, doi:10.1093/icesjms/fsv110, 2015.

Schlegel, R. W., Darmaraki, S., Benthuysen, J. A., Filbee-Dexter, K., and Oliver, E. C.: Marine cold-spells, *Progress in Oceanography*, *198*, 102684, doi.org/10.1101/2021.10.18.464880, 2021.

Serre-Fredj, L., Jacqueline, F., Navon, M., Izabel, G., Chasselin, L., Jolly, O., ... and Claquin, P.: Coupling high frequency monitoring and bioassay experiments to investigate a harmful algal bloom in the Bay of Seine (French-English Channel), *Marine Pollution Bulletin*, *168*, 112387, doi:10.1016/j.marpolbul.2021.112387, 2021.

Smetacek, V., & Cloern, J. E.: On phytoplankton trends, *Science*, *319*(5868), 1346-1348, doi: 10.1126/science.1151330, 2008.

Sommer, U., Adrian, R., De Senerpont Domis, L., Elser, J. J., Gaedke, U., Ibelings, B., Jeppesen, E., Lürling, M., Molinero, J. C., Mooij, W. M., van Donk, E., and Winder, M.: Beyond the Plankton Ecology Group (PEG) model: mechanisms driving plankton succession, *Annual review of ecology, evolution, and systematics*, *43*, 429-448, doi:10.1146/annurev-ecolsys-110411-160251, 2012.

Stockwell, J. D., Doubek, J. P., Adrian, R., Anneville, O., Carey, C. C., Carvalho, L., ... and Wilson, H. L.: Storm impacts on phytoplankton community dynamics in lakes, *Global change biology*, *26*(5), 2756-2784, doi:10.1111/gcb.15033, 2020.

Sverdrup, H.: On vernal blooming of phytoplankton, *Conseil Exp. Mer*, *18*, 287-295, 1953.

Thyssen, M., Tarran, G. A., Zubkov, M. V., Holland, R. J., Grégori, G., Burkill, P. H., and Denis, M.: The emergence of automated high-frequency flow cytometry: revealing temporal and spatial phytoplankton variability, *Journal of plankton research*, *30*(3), 333-343, doi:10.1093/plankt/fbn005, 2008.

Tian, T., Merico, A., Su, J., Staneva, J., Wiltshire, K., and Wirtz, K.: Importance of resuspended sediment dynamics for the phytoplankton spring bloom in a coastal marine ecosystem, *Journal of Sea Research*, *62*(4), 214-228, doi:10.1016/j.seares.2009.04.001, 2009.

Tian, T., Su, J., Flöser, G., Wiltshire, K., and Wirtz, K.: Factors controlling the onset of spring blooms in the German Bight 2002–2005: light, wind and stratification, *Continental Shelf Research*, *31*(10), 1140-1148, doi:10.1016/j.csr.2011.04.008, 2011.

Townsend, D. W., Cammen, L. M., Holligan, P. M., Campbell, D. E., and Pettigrew, N. R.: Causes and consequences of variability in the timing of spring phytoplankton blooms, *Deep Sea Research Part I: Oceanographic Research Papers*, *41*(5-6), 747-765, doi:10.1016/0967-0637(94)90075-2, 1994.

Trombetta, T., Vidussi, F., Mas, S., Parin, D., Simier, M., and Mostajir, B. : Water temperature drives phytoplankton blooms in coastal waters, *PloS one*, *14*(4), e0214933, doi:10.1371/journal.pone.0214933, 2019.

Wiltshire, K. H., Malzahn, A. M., Wirtz, K., Greve, W., Janisch, S., Mangelsdorf, P., ... and Boersma, M.: Resilience of North Sea phytoplankton spring bloom dynamics: An analysis of long-term data at Helgoland Roads, *Limnology and Oceanography*, *53*(4), 1294-1302, doi:10.4319/lo.2008.53.4.1294, 2008.

Wiltshire, K. H., Boersma, M., Carstens, K., Kraberg, A. C., Peters, S., and Scharfe, M.: Control of phytoplankton in a shelf sea: determination of the main drivers based on the Helgoland Roads Time Series, *Journal of Sea Research*, 105, 42-52, doi:10.1016/j.seares.2015.06.022, 2015.

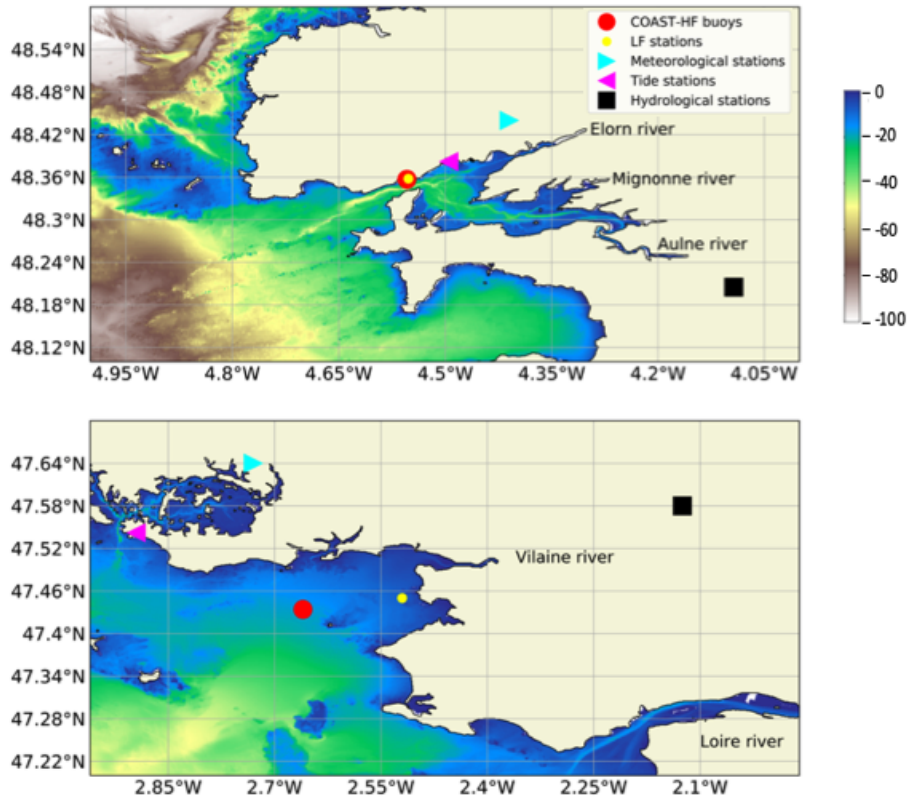

Figure 1: Location of the sampling sites: COAST-HF-Iroise and COAST-HF-Molit buoys (red circles); SOMLIT-Brest and REPHY-Loscolo sampling stations (yellow circles); Brest and Crouesty tide gauge stations (blue triangles); Guipavas and Vannes-Séné meteorological stations (purple triangles); hydrological stations of the Aulne and Vilaine rivers (black squares) with the Loire station off the map.

Parameters	Bay of Brest	Bay of Vilaine
Dissolved O_2 *(mg L^{-1})*	9	10
Mesozooplankton *(µmolN L^{-1})*	0.05	0.1
Microzooplankton *(µmolN L^{-1})*	0.05	0.05
Dinoflagellates *(µmolN L^{-1})*	0.05	0.1
Diatoms *(µmolN L^{-1})*	0.5	0.5
Soluble reactive phosphorus *(µmol L^{-1})*	0.5	0.8
Silicic acid *(µmol L^{-1})*	10	30
Nitrate *(µmol L^{-1})*	16	30
Ammonium *(µmol L^{-1})*	0.5	0.25
Coarse sand *(g L^{-1})*	0	0
Fine sand *(g L^{-1})*	0	0

Mud *(g L^{-1})*	0.03	0.05

Table 1: Initial conditions in the water column for the MARS-1DV model for the beginning of the simulation on the February 15th.

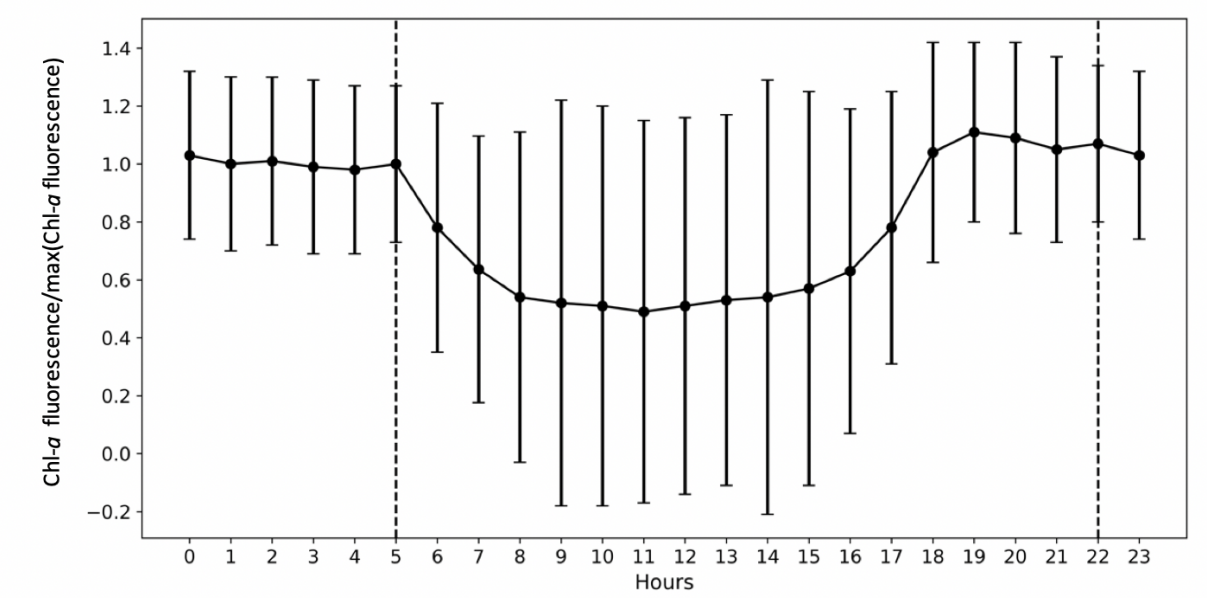

Figure 2: Importance of the Quenching effect on Chl-*a* fluorescence is represented by COAST-HF-Iroise data from 2000 to 2019. The standard deviation is represented by vertical black bars. The dashed lines represent the beginning and end of the selected values for the rest of the study from 10 pm to 5 am.

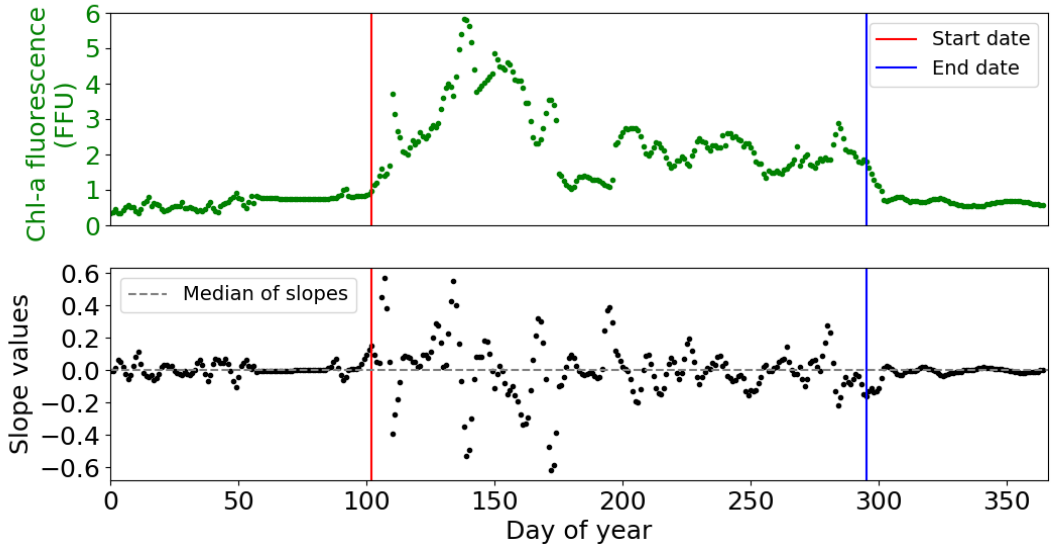

Figure 3: Example of detection of the start (red line) and end (blue line) of the phytoplankton growing period in 2001 at COAST-HF-Iroise. The threshold value - median of slopes - is represented by a dotted grey line.

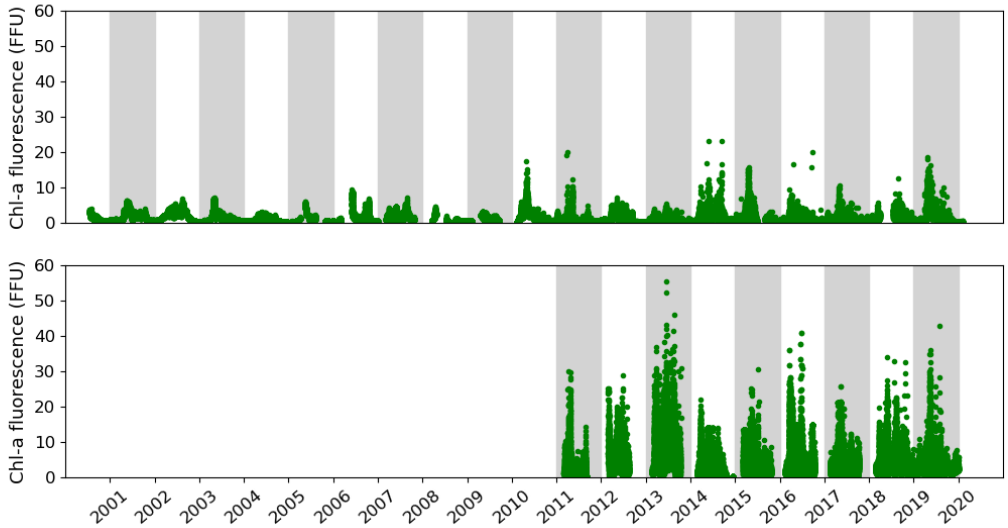

Figure 4: Temporal changes in the *in situ* Chl-*a* fluorescence measured in the Bay of Brest (top) and the Bay of Vilaine (bottom).

	Start date (Day of year)	**End date** (Day of year)	**Duration** (Days)	**Cumulative Chl-*a* fluorescence** (FFU)
	*Min - **Median** - Max*	*Min - **Median** - Max*	*Min - **Median** - Max*	*Min - **Median** - Max*
Bay of Brest (2001-2019)	50 - **69** - 102	253 - **274** - 308	165 - **200** - 256	217 - **364** - 567
Bay of Vilaine (2011-2019)	53 - **68** - 93	218 - **269** - 316	165 - **179** - 239	276 - **582** - 1406

Table 2: Global characteristics of the phytoplankton growing period in the Bay of Brest and in the Bay of Vilaine.

(a)

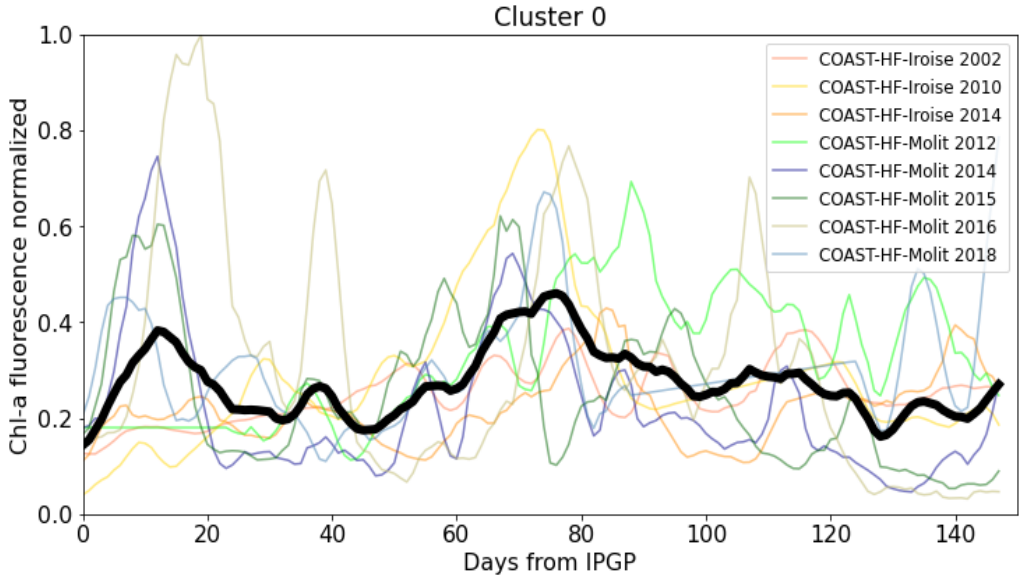

(b)

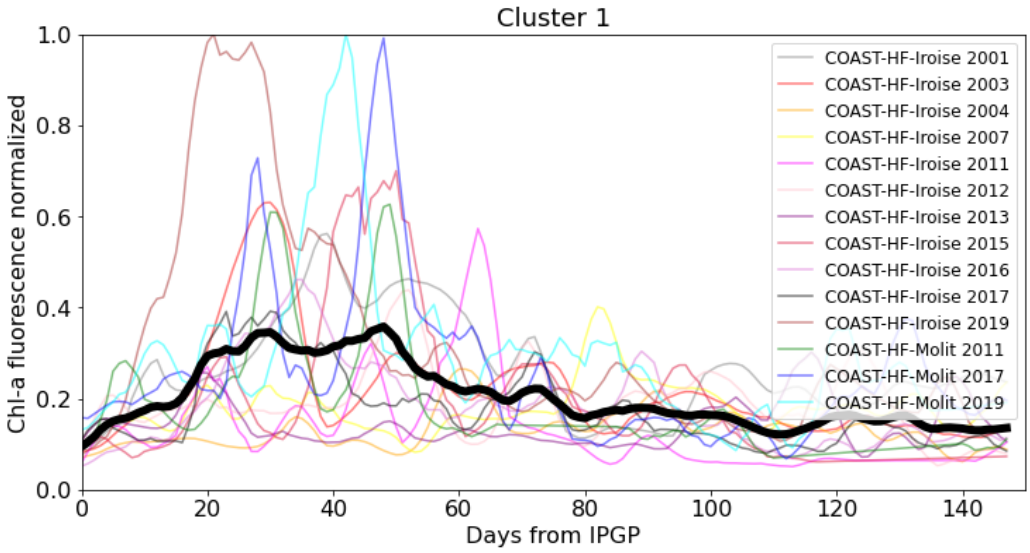

Figure 5: (a) Cluster 0 and (b) cluster 1 representative of the patterns of the phytoplankton growing period observed in both bays. The median pattern is drawn in bold.

Year	2001	2002	2003	2004	2005	2006	2007	2008	2009	2010	2011	2012	2013	2014	2015	2016	2017	2018	2019
Bay of Brest COAST-HF-Iroise	1	0	1	1			1			0	1	1	1	0	1	1	1		1
Bay of Vilaine COAST-HF-Molit											1	0	X	0	0	0	1	0	1

Table 3: Cluster group assigned to each annual phytoplankton growing period on both sites. Grey boxes represent years with missing data. The cross represents the year 2013 of the Bay of Vilaine not considered.

(a)

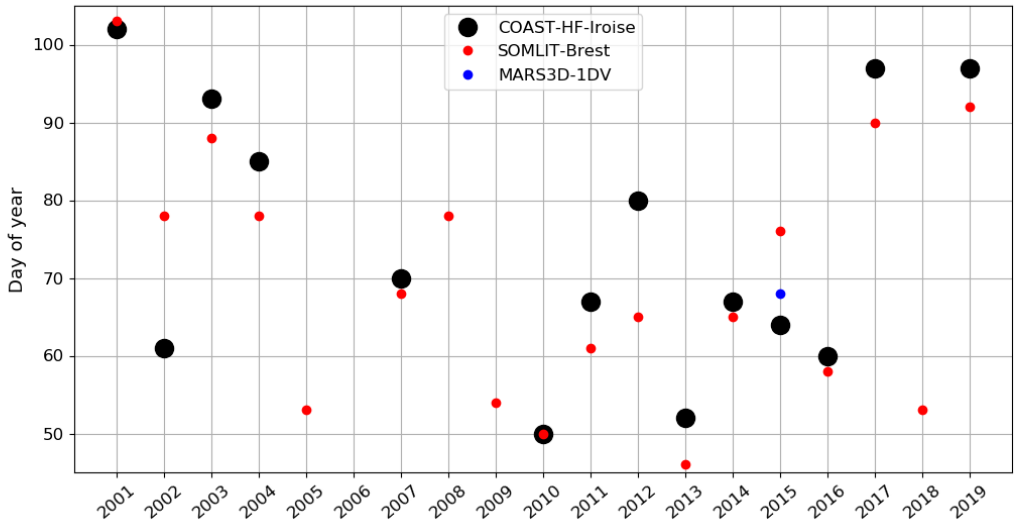

(b)

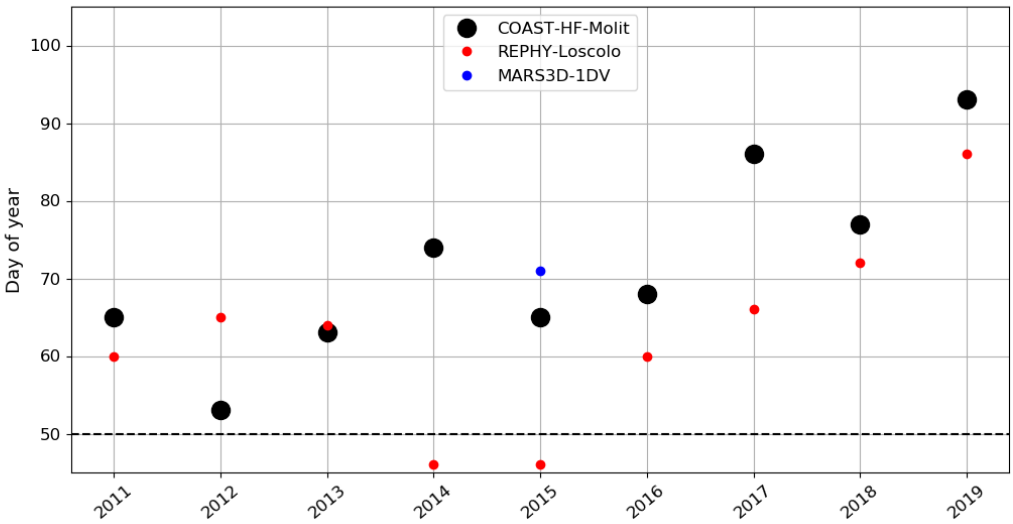

Figure 6: Changes in the IPGP date in (a) the Bay of Brest and (b) the Bay of Vilaine are determined with high-frequency time series (black circles), low-frequency time series (red circles) and with the model (blue circle). The dotted black line represents the date of the COAST-HF-Molit buoy deployment.

(a)

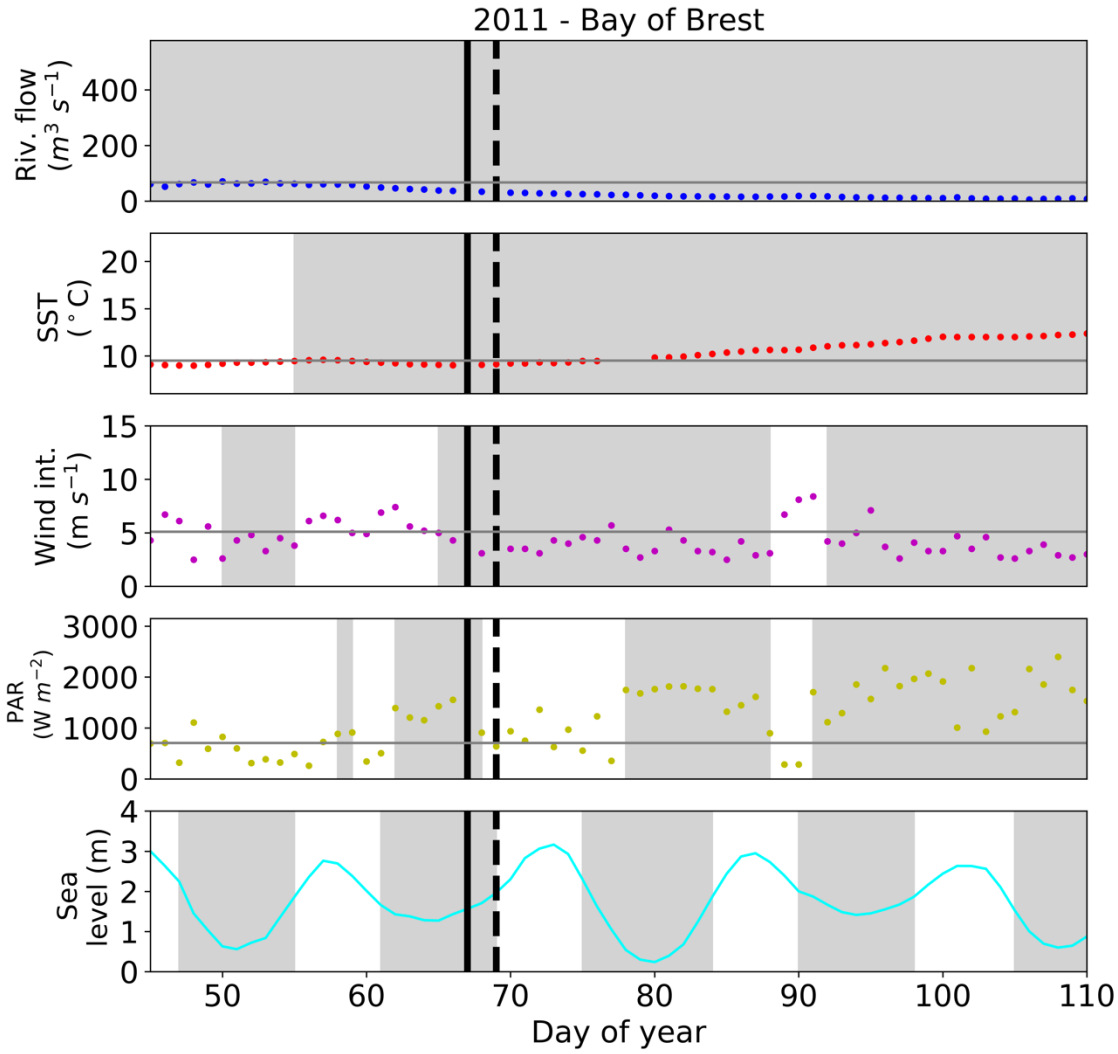
2011 - Bay of Brest
Riv. flow ($m^3\ s^{-1}$)
400
200
0
SST (°C)
20
15
10
Wind int. ($m\ s^{-1}$)
15
10
5
0
PAR ($W\ m^{-2}$)
3000
2000
1000
0
Sea level (m)
4
3
2
1
0
50
60
70
80
90
100
110
Day of year

(b)

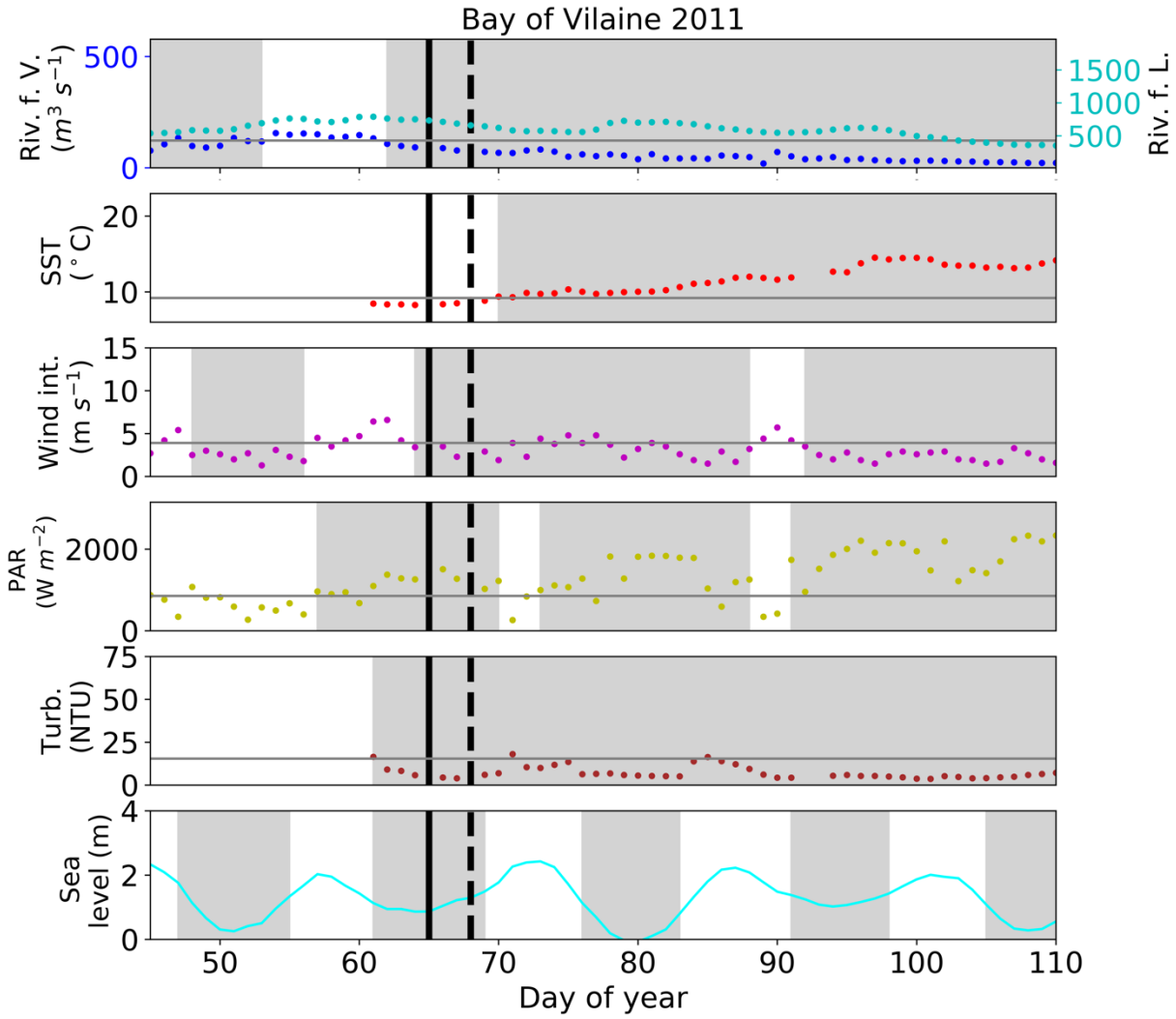
Bay of Vilaine 2011
Riv. f. V. (m^3 s^{-1})
500
0
1500
1000
500
Riv. f. L.
SST (°C)
20
10
Wind int. (m s^{-1})
15
10
5
0
PAR (W m^{-2})
2000
0
Turb. (NTU)
75
50
25
0
Sea level (m)
4
2
0
50
60
70
80
90
100
110
Day of year

(c)

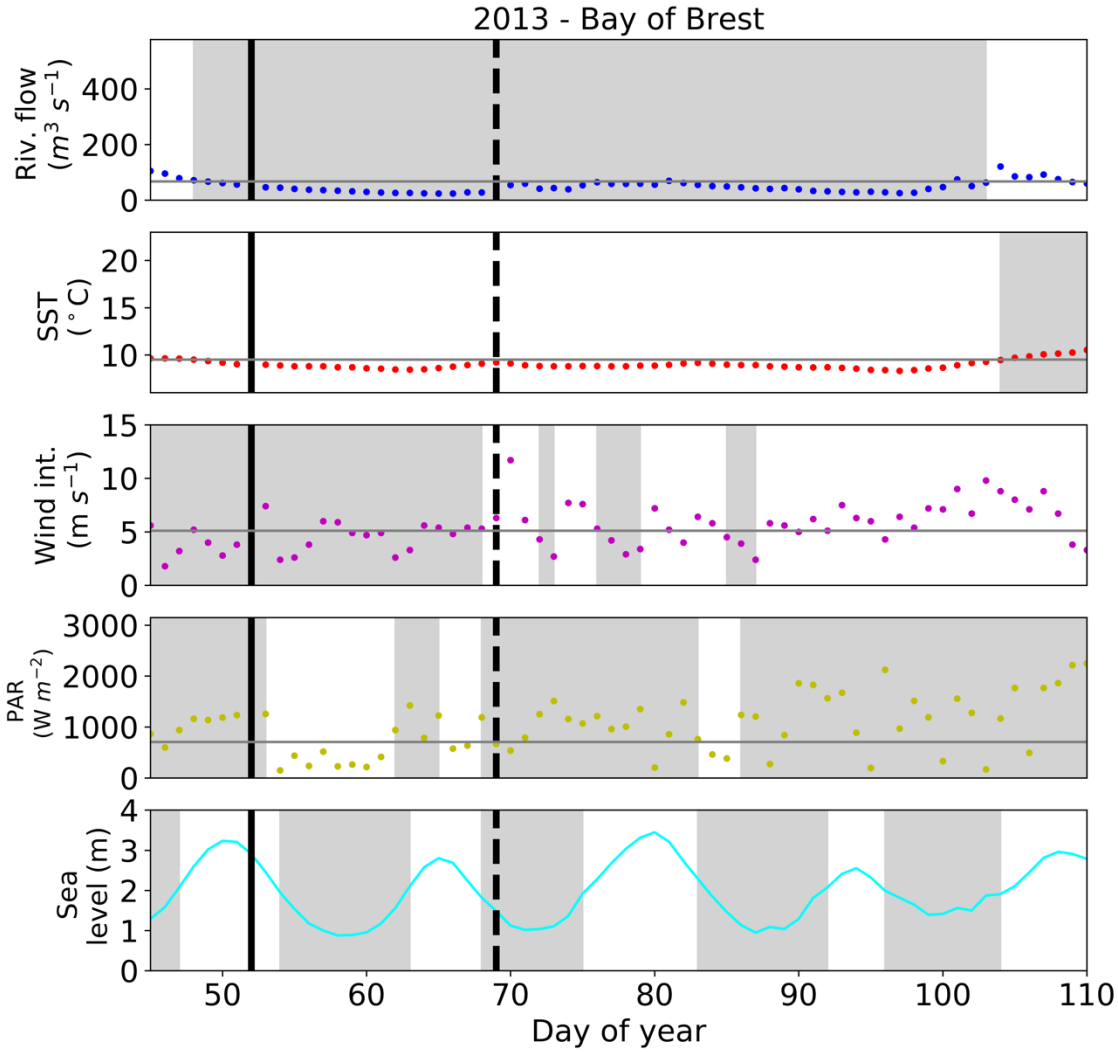
2013 - Bay of Brest
Riv. flow ($m^3\ s^{-1}$)
400
200
0
SST (°C)
20
15
10
Wind int. ($m\ s^{-1}$)
15
10
5
0
PAR ($W\ m^{-2}$)
3000
2000
1000
0
Sea level (m)
4
3
2
1
0
50
60
70
80
90
100
110
Day of year

(d)

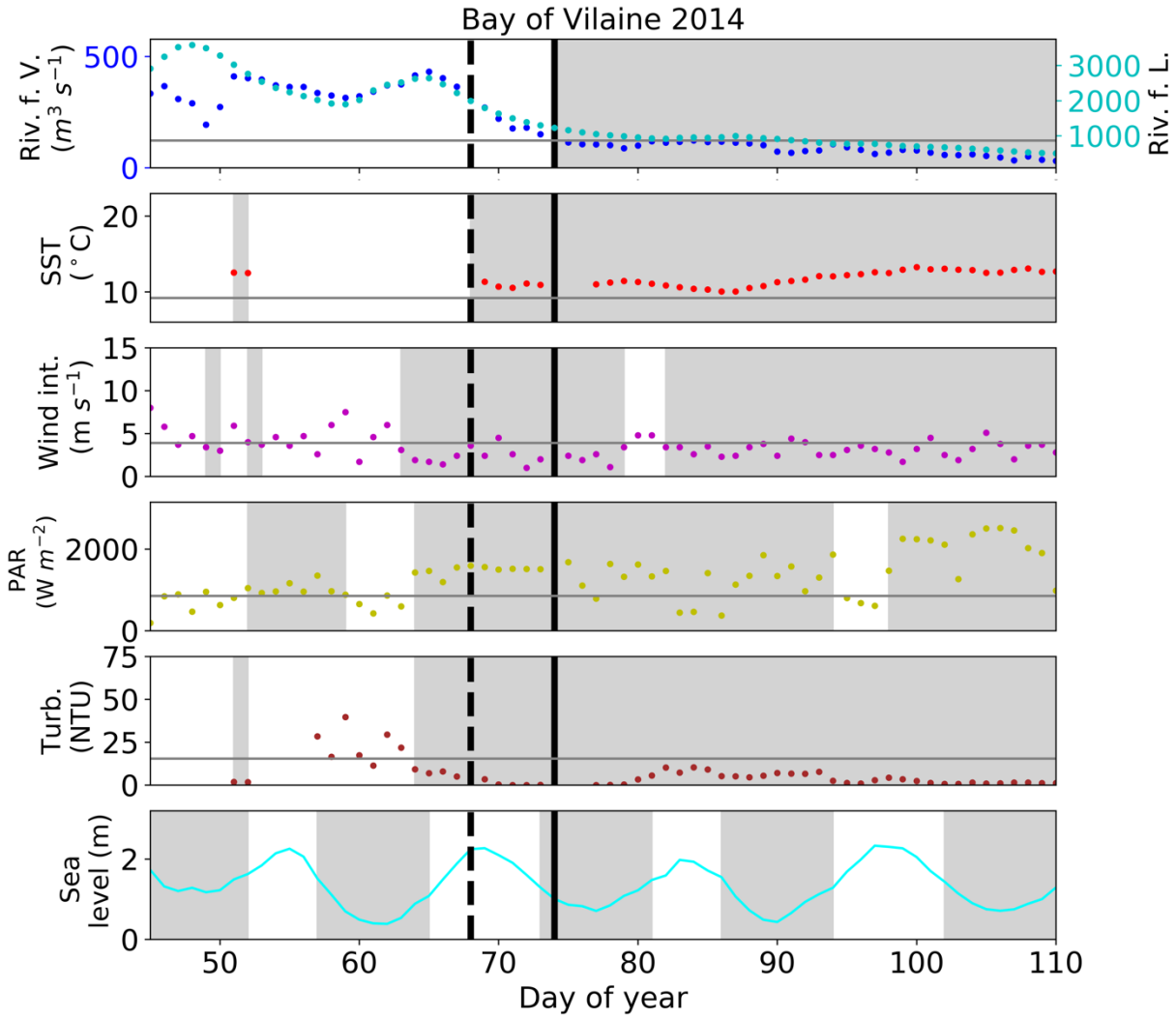

Figure 7: IPGP dates and environmental drivers: flow of the Aulne, Vilaine and Loire rivers, Sea Surface Temperature (SST), wind intensity, PAR, turbidity and sea level at high tide. Illustrations in 2011 for a mean IPGP date in (a) the Bay of Brest and (b) the Bay of Vilaine; in 2013 for an early IPGP date in (c) the Bay of Brest; in 2014 for a late IPGP date in (d) the Bay of Vilaine. The mean IPGP date of each bay is represented by a dotted black line and the IPGP date of the year is represented by a straight black line. Thresholds of each environmental driver are represented by grey vertical lines corresponding to the mean conditions calculated 30 days around the IPGP date. Grey areas are time periods favorable to IPGP.

	Bay of Brest (2001-2019)	Bay of Vilaine (2011-2019)
	*Min - **Median** - Max*	*Min - **Median** - Max*
River flow ($m^3\ s^{-1}$)	13 - **46** - 100	36 - **96** - 205
SST (°C)	8 - **10** - 12	8 - **10** - 11
Wind intensity ($m\ s^{-1}$)	1 - **3** - 6	1 - **3** - 4
PAR ($W\ m^{-2}$)	915 - **1373** - 2220	814 - **1341** - 1939
Turbidity (NTU)	1 - **7** - 21	0 - **7** - 22
Sea level (m)	0.5 - **1.6** - 2.9	0.6 - **0.9** - 1.6
PO_4 (µmol/L)	0.1 – **0.4** – 0.6	0.1 – **0.8** – 1.4
DIN (µmol/L)	8 – **20** – 38	25 - **57** - 244
$Si(OH)_4$ (µmol/L)	4 - **8** - 16	8 - **38** - 112

Table 4: Characteristics of environmental drivers at the date of IPGP in the Bay of Brest and in the Bay of Vilaine.

(a)

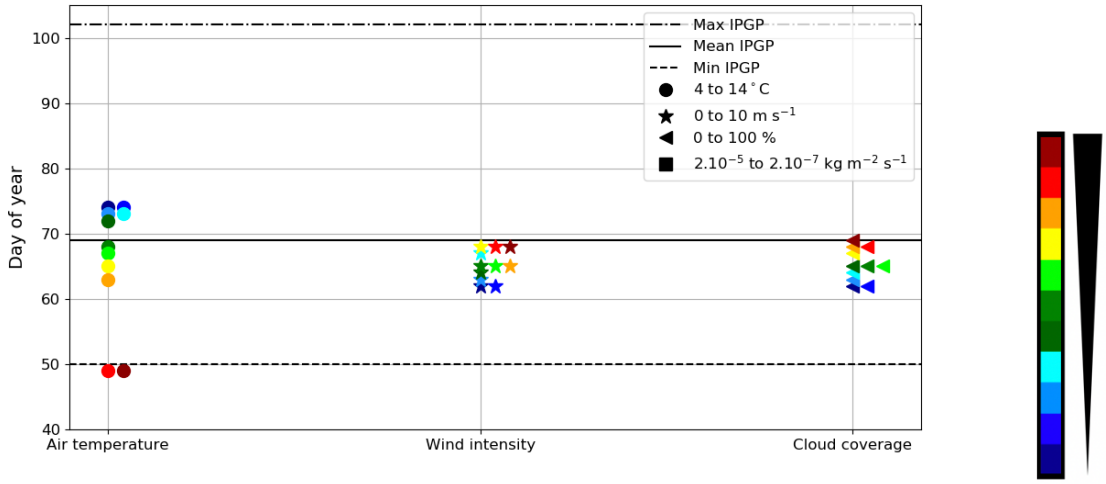

(b)

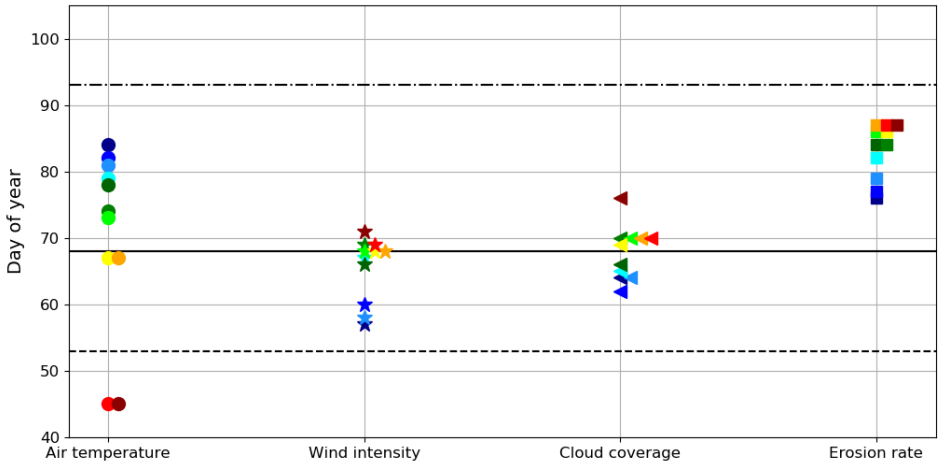

Figure 8: Impact of the variation of environmental drivers on the date of IPGP in (a) the Bay of Brest and (b) the Bay of Vilaine. Steps of: 1°C for the air temperature, 1 m s^{-1} for the wind intensity, 10 % for the cloud coverage and 0.0000036 kg m^{-2} s^{-1} for the erosion rate equivalent to a variation of suspended matter between 0.02 and 0.08 mg L^{-1} at IPGP.

Experiment	Air temperature (°C)	Wind intensity (m s^{-1})	Cloud coverage (%)	Erosion rate (kg m^{-2} s^{-1})	Simulated IPGP Bay of Brest (days)	Simulated IPGP Bay of Vilaine (days)
1	**4**	**3**	**70**	2.10^{-6}	+5	+16
2	**14**	**3**	**70**	2.10^{-6}	-20	-23
3	**10**	**0**	**70**	2.10^{-6}	-1	-11
4	**10**	**10**	**70**	2.10^{-6}	-7	+3
5	**10**	**3**	**0**	2.10^{-6}	=	-4
6	**10**	**3**	**100**	2.10^{-6}	-7	+8
7	10	3	70	2.10^{-7}		+8
8	10	3	70	2.10^{-5}		+19
A	**4**	**10**	**100**	2.10^{-5}	+9	+64
B	**4**	**10**	**70**	2.10^{-6}	+5	+17
C	**4**	**3**	**100**	2.10^{-6}	+5	+28
D	**10**	**10**	**100**	2.10^{-6}	=	+6
E	4	10	70	2.10^{-5}		+48
F	4	3	100	2.10^{-5}		+46
G	10	10	100	2.10^{-5}		+34
H	10	3	100	2.10^{-5}		+19
I	10	10	70	2.10^{-5}		+29
J	4	3	70	2.10^{-5}		+36
K	**14**	**0**	**0**	2.10^{-7}	-20	-11
L	**14**	**0**	**70**	2.10^{-7}	-21	-11
M	**14**	**3**	**0**	2.10^{-7}	-20	-11
N	**10**	**0**	**0**	2.10^{-7}	-11	-11

Table 5: Assumptions are explored in the 1DV model for environmental parameters independently (1-8) and with combined effect (A-N) with the modified values (grey background) and text in bold for the Bay of Brest only (+ for later IPGP, - for earlier IPGP, = for equal IPGP) with IPGP equal the mean observed IPGP of day 68.

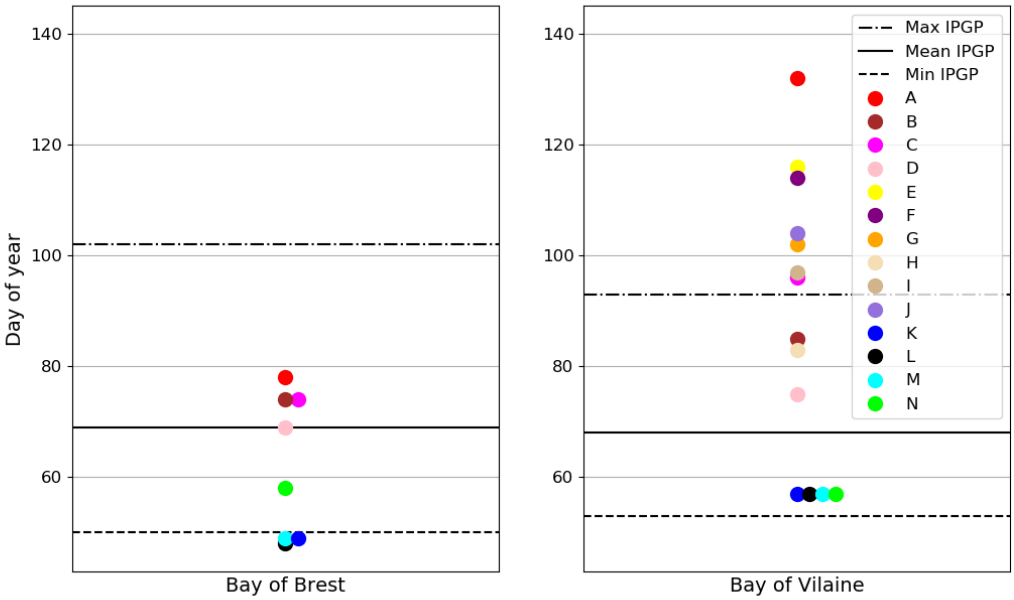

Figure 9: Influence of combined environmental parameters for the MARS-1DV model in both bays (Bay of Brest - left and Bay of Vilaine - right) with detailed experiments in Table 2.

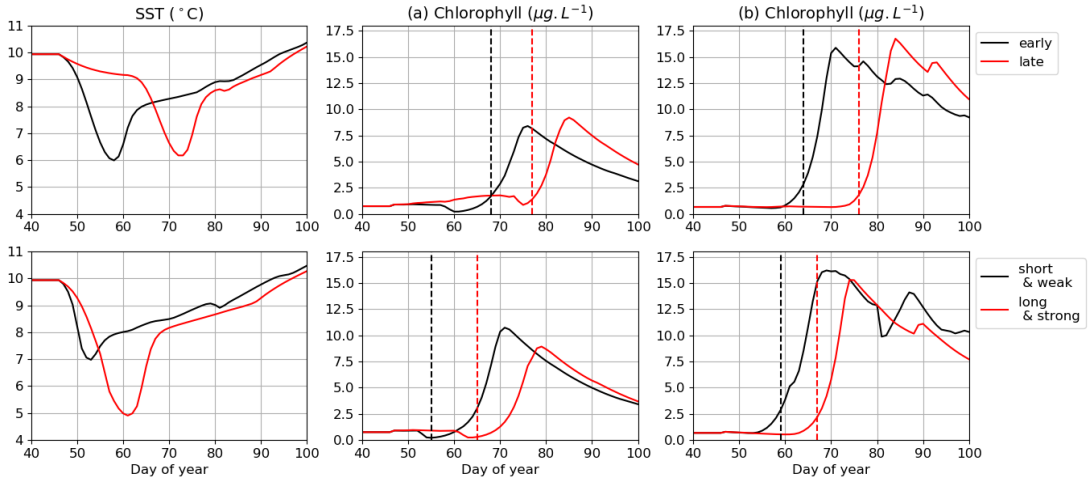

Figure 10: Impact of cold spells on the IPGP date simulated in (a) the Bay of Brest and (b) the Bay of Vilaine. Four conditions of cold spells are explored: an early (mid-February), a late (end of February), a short (8 days) and a long (20 days). The IPGP dates are represented by dotted lines.